Earth-Science Reviews 252 (2024) 104761

Contents lists available at ScienceDirect

Earth-Science Reviews

journal homepage: www.elsevier.com/locate/earscirev

# Tracing the subduction and accretion history of the trench-arc-basin system in the Chinese Eastern Tianshan: Insights from Paleozoic magmatic and crustal evolution

Long Du [a,b,**], Xiaoping Long [b,*], Chao Yuan [c], Yunying Zhang [d], Zongying Huang [c], Hongli Zhu [e]

[a] Research Center of Continental Dynamics, College of Earth Science and Engineering, Shandong University of Science and Technology, Qingdao 266590, China
[b] State Key Laboratory of Continental Dynamics, Department of Geology, Northwest University, Xi'an 710069, China
[c] State Key Laboratory of Isotope Geochemistry, Guangzhou Institute of Geochemistry, Chinese Academy of Sciences, Guangzhou 510640, China
[d] Key Laboratory of Ocean and Marginal Sea Geology, South China Sea Institute of Oceanology, Innovation Academy of South China Sea Ecology and Environmental Engineering, Chinese Academy of Sciences, Guangzhou 510301, China
[e] Center of Deep Sea Research, Institute of Oceanology, Chinese Academy of Sciences, Qingdao 266071, China

ARTICLE INFO

*Keywords:*
Central Asian Orogenic Belt (CAOB)
Eastern Tianshan
Kangguer Ocean
Igneous rocks
Crustal evolution

ABSTRACT

Accretionary orogens function as crucial sites for the generation of arc igneous rocks and continental crust, but the spatial and temporal distribution of arc igneous rocks and the link between the arc magmatic processes and crust generation within individual orogens remains poorly constrained. To address this issue, we have summarized published geochemical and zircon isotopic data for Paleozoic (~460–280 Ma) mafic–intermediate–felsic igneous rocks within five individual belts from the Chinese Eastern Tianshan of the southern Central Asian Orogenic Belt (CAOB), which aim to explore the variations in magma sources (juvenile or reworked crust) and crustal thickness in response to tectonic and crustal evolution over time. This summary highlights the systematic variation in elemental and isotopic signatures of magmas in the Eastern Tianshan and makes it possible to quantitatively evaluate the crustal evolution and tectonic switch patterns. Repeated tectonic switches of the Eastern Tianshan trench-arc-basin system during subduction of the Kangguer oceanic plate appear to have occurred in two phases of the northern trench advance (ca. 460–381 Ma and 330–301 Ma, respectively) and the intervening trench retreat (ca. 380–331 Ma), as well as seem to have happened in the southern trench of the Kangguer Ocean with trench southward advance and northward retreat at ca. 360–331 Ma and 330–301 Ma, respectively. The estimated crustal growth in the Eastern Tianshan various from trench advance accompanied by significant crustal thickening (i.e., northern trench advance at ca. 460–421 Ma and southern trench advance at ca. 360–331 Ma, respectively) to northern trench retreat with crustal thinning (ca. 380–331 Ma). Most of the magma in the Eastern Tianshan was generated by crustal reworking or mixing.

## 1. Introduction

The growth and reworking of the continental crust through time has long been a subject of debate (e.g., Armstrong, 1981; Condie, 1998; Belousova et al., 2010; Dhuime et al., 2012; Spencer et al., 2019; Wang et al., 2023). Considering that continental crust has a bulk andesitic to dacitic composition (Rudnick and Gao, 2014), most previous studies have focused on continental arcs, such as the North and South American Cordillera and the Australian Tasmanides, which developed the idea that the generation of crust takes place mainly during the extensional stage of a continental arc (Kemp et al., 2009; Chapman and Ducea, 2019; Spencer et al., 2019). However, whether the results of such studies can be applied to island arc magmatism in accretionary orogens remains unclear.

Accretionary orogens form at sites of intra-oceanic subduction and continental margins, where extensive magmatism and crustal growth takes place as a consequence of continuing subduction and accretion (Reymer and Schubert, 1986; Beltrando et al., 2007; Condie, 2007;

* Corresponding author.
** Corresponding author at: Research Center of Continental Dynamics, College of Earth Science and Engineering, Shandong University of Science and Technology, Qingdao 266590, China.
*E-mail addresses:* dulong@sdust.edu.cn (L. Du), longxp@nwu.edu.cn (X. Long).

https://doi.org/10.1016/j.earscirev.2024.104761
Received 30 November 2023; Received in revised form 19 February 2024; Accepted 25 March 2024
Available online 1 April 2024

Cawood et al., 2009). There is increasing evidence that crustal growth takes place in different ways in different accretionary orogens, including outward growth of juvenile magmatic arcs, and vertical growth of mantle input during extensional episodes (Sengör et al., 1993; Jahn et al., 2004; Cawood et al., 2009; Kröner et al., 2014; Tang et al., 2017; Gong et al., 2023; Wang et al., 2023), which differs from the opinion that the production of crust takes place mainly at the extensional stage of a continental arc (Kemp et al., 2009; Chapman and Ducea, 2019; Spencer et al., 2019). The key issues in this paradox are the relative roles of crustal growth along with crustal thickening during advancing subduction or accompanied by crustal thinning at retreating subduction, as well as the relative characters of juvenile crustal growth (i.e., crust derived from the mantle) and crustal reworking (i.e., remelting of older crust) in the Earth's history and especially during the Phanerozoic (Armstrong, 1981; Belousova et al., 2009; Dhuime et al., 2012; Kröner et al., 2014; Tang et al., 2017; Wang et al., 2023).

As the largest Phanerozoic accretionary orogeny worldwide, the Central Asian Orogenic Belt (CAOB), also known as Altaids (Sengör et al., 1993; Sengör and Natalin, 1996; Wilhem et al., 2012) and Central Asian Mobile Belt (Jahn et al., 2004), located between the European, Siberian, Tarim, and North China Cratons (Fig. 1A; Sengör et al., 1993; Xiao et al., 2015; Yang et al., 2015), is generally considered as one of the major sites of juvenile crust production on Earth (Sengör et al., 1993; Windley et al., 2007; Cawood et al., 2013; Kröner et al., 2014; Tang et al., 2017; Wang et al., 2022, 2023). The preserved part of the CAOB records complex and multiple subduction and accretion of various tectonic domains such as arc–back-arc systems, accretionary prisms, ophiolitic mélanges, and microcontinents within the Paleo-Asian Ocean, marking the transition from the Pangea supercontinent to the evolving Eurasian continent (Windley et al., 1990; Sengör et al., 1993; Xiao et al., 2015; Kröner et al., 2017; Huang et al., 2020; Liu et al., 2021; Li et al., 2022; Wang et al., 2023).

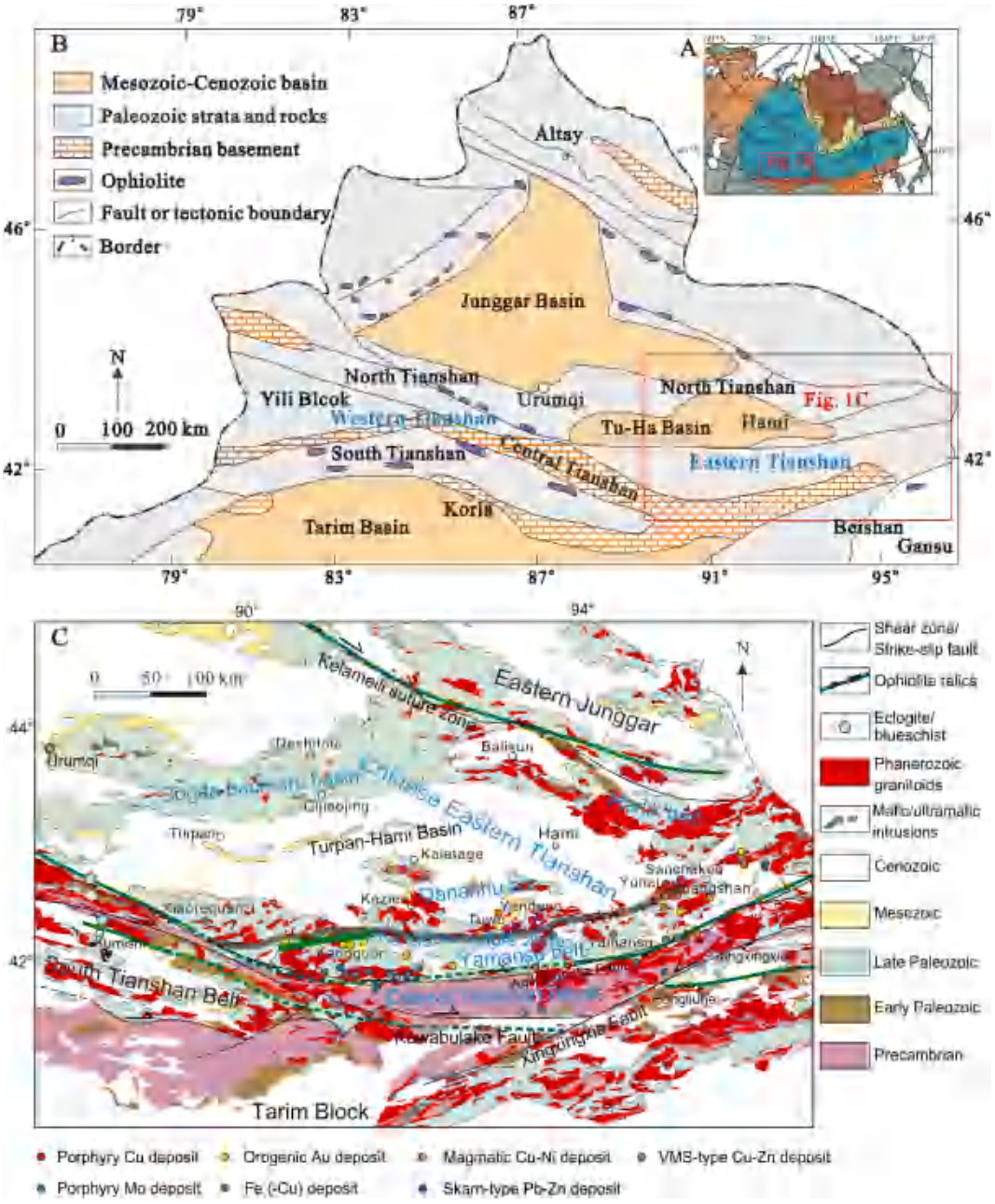


**Fig. 1.** (A) Sketch map of the CAOB and the surrounding Cratons (modified from Jahn et al., 2000). (B) Sketch map of the North Xinjiang (after Gao et al., 2009). (C) Geological map of the Chinese Eastern Tianshan (after Han and Zhao, 2018).

The Chinese Eastern Tianshan occupies the southernmost CAOB and contains the essential components of a typical accretionary orogen such as island arcs, ophiolites, continental margin arcs, microcontinents, and accretionary wedges (Fig. 1B and C; Xiao et al., 2004; Windley et al., 1990, 2007; Wang et al., 2021; Mao et al., 2022a, 2022b; Zhang et al., 2022). It formed by the successive lateral accretion of island arcs, continental margin arcs, ophiolites, and accretionary complexes, as well as by the vertical addition of significant volumes of magmas in accretionary, post-collisional, and intraplate settings (Xiao et al., 2004; Windley et al., 1990, 2007; Zhang et al., 2018; Wang et al., 2022; Gong et al., 2023). Hence, it is critical to understand the timing and nature of the multi-stage magmatism so as to decipher the subduction and accretion history, crustal thickness, and links with crustal growth and reworking of the CAOB (Sengör et al., 1993; Jahn et al., 2000; Xiao et al., 2004, 2008; Wilhem et al., 2012; Yang et al., 2015; Wang et al., 2022, 2023). In fact, the amalgamation history in the Eastern Tianshan has been one of the focal themes in recent years, but remains controversial (Xiao et al., 2004, 2008; Zhang et al., 2018; Du et al., 2021; Mao et al., 2022a; Wang et al., 2022; Gong et al., 2023). One reason for the debate centers on the pattern and amount of juvenile crust generated in the CAOB, as well as generated in the Eastern Tianshan, is highly variable (Jahn et al., 2000, 2004; Kröner et al., 2014, 2017; Tang et al., 2017; Wang et al., 2022, 2023; Gong et al., 2023). Another reason for the debate may have been that most of those studies were focused on the investigation of particular aspects in localized areas or limited times and therefore did not provide a comprehensive analysis at the regional scale.

This paper focuses on the Eastern Tianshan, which provides a record of igneous activity throughout most of the Paleozoic (Tang et al., 2017; Wang et al., 2022; Gong et al., 2023). We compile a data set of the whole-rock geochemical and zircon U-Pb and Lu-Hf isotopic compositions of magmatic rocks of the Eastern Tianshan (Tables S1–5). We take the evolution of magma sources (juvenile vs. reworked crust) and crust thickness over time as the main reference indexes to improve understanding of the subduction, accretion, and crustal evolution history of the southern CAOB.

## 2. Geological background and tectonic division of the Chinese Eastern Tianshan

The Chinese Tianshan is separated from the Junggar terrane to the north and from the Tarim Craton to the south (Fig. 1B). It is a complex collage of island arcs, basins, oceanic remnants, accretionary complexes, and microcontinents (Windley et al., 1990; Xiao et al., 2004; Charvet et al., 2007; Kröner et al., 2017; Han and Zhao, 2018; Huang et al., 2020). It can be geographically divided into the Eastern and Western Tianshan by a transection roughly along the Urumqi–Korla road. This study concentrates on the Chinese Eastern Tianshan, from north to south, containing the Harlik arc, the Bogda back-arc basin, the Dananhu arc, the Kanggur accretionary complex, the Yamansu arc, and the eastern part of the Central Tianshan block (Fig. 1C).

### 2.1. The Harlik belt

The nearly NW–SE trending Harlik belt separates from the Junggar basin to the northeast and from the Turfan-Hami basin to the southwest (Fig. 1C). The Harlik terrane is mainly composed of Paleozoic strata, with some Jurassic strata exposed on the southern foothill (Fig. 2; BGMRXUAR, 1993; Zhao et al., 2014; Chen et al., 2020). The oldest sedimentary strata in the Harlik terrane are the Ordovician to Silurian Huangcaopo Group, which are exposed along the northeastern Harlik Mountain and consist of slate, metasandstone, conglomerate, and minor pyroclastic rock of the bathyal facies and littoral-neritic clastic rocks (Long et al., 2012; Zhao et al., 2022). The Devonian strata are locally distributed in the Harlik Mountain and are composed of grey metaclastic rocks and limestones (Ma, 1999; Deng et al., 2016). The Carboniferous strata unconformably overlie the Devonian strata, and they are the most widespread Paleozoic strata in the Harlik belt and mainly consist of marine-terrigenous facies coarse clastic rocks (Ma, 1999; Zhao et al., 2022). Finally, Permian volcanic strata are well-developed in the western part of the Harlik Mountain (BGMRXUAR, 1993; Chen et al., 2020).

In addition, geochronological studies have suggested that mafic–intermediate–felsic magmatic rocks in the Harlik belt were

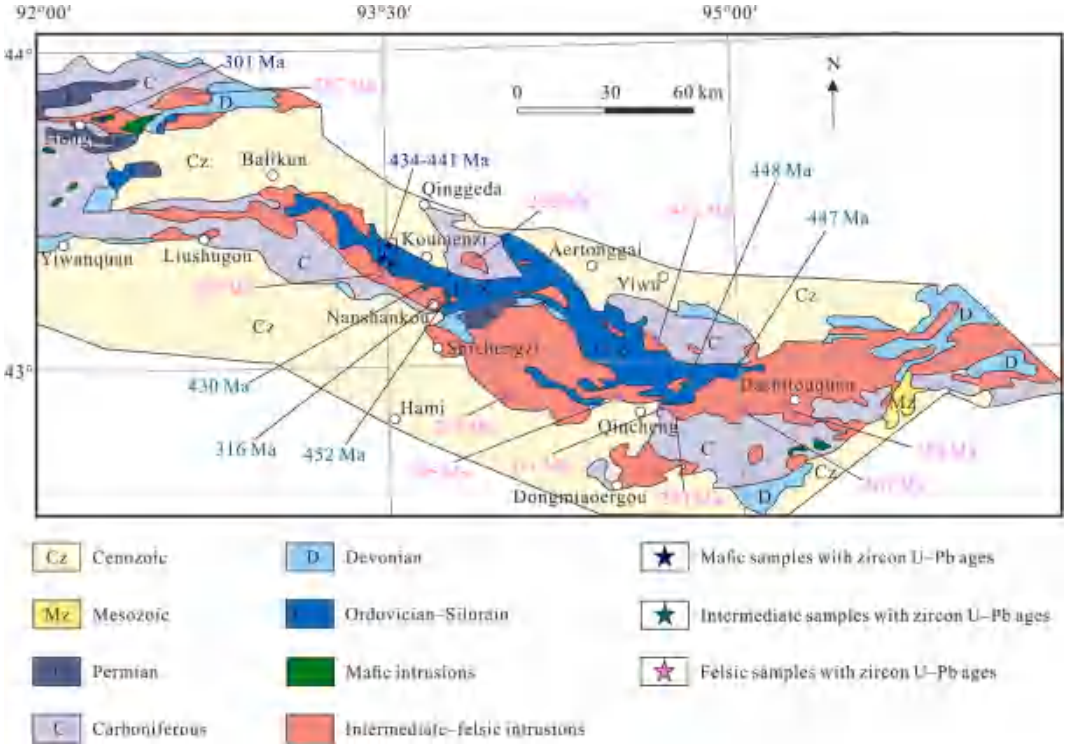


**Fig. 2.** Geological map of the Harlik belt (modified after Zhao et al., 2014). Detailed descriptions of the mafic–intermediate–felsic rocks can be found in Table S1.

dominantly produced in the Late Ordovician to Early Silurian and Late Carboniferous to Early Permian, but few in the Late Silurian to Early Carboniferous (Figs. 2 and 3A; Table S1; Cao et al., 2006; Guo et al., 2006; Yuan et al., 2010; Ma et al., 2015; Du et al., 2018a; Zhao et al., 2022).

### 2.2. The Bogda belt

The Bogda belt, with the Harlik arc to the north and the Dananhu arc to the south, have been proposed as a united arc–back-arc assemblage (Xiao et al., 2004; Zhang et al., 2018; Du et al., 2023). The oldest sedimentary strata in the Bogda belt are dominated by Devonian marine-terrigenous tuffaceous sandstone and volcanic rock (Fig. 4; BGMRXUAR, 1993; Zhao et al., 2014; Xie et al., 2016). The Carboniferous strata are in fault contact with the Devonian rocks and comprise three formations, namely, the Lower Carboniferous Qijiaojing Formation, the Upper Carboniferous Liushugou and Qijiagou Formations (Chen et al., 2013; Xie et al., 2016). The Lower Carboniferous Formation consists mainly of marine volcanic ignimbrite, tuffaceous sandstone, and bimodal volcanic lava, while the Upper Carboniferous Formation is dominated by large volumes of shallow-marine pillow basaltic and rhyolite lava, and felsic ignimbrite, with minor sandstone and siltstone (BGMRXUAR, 1993;

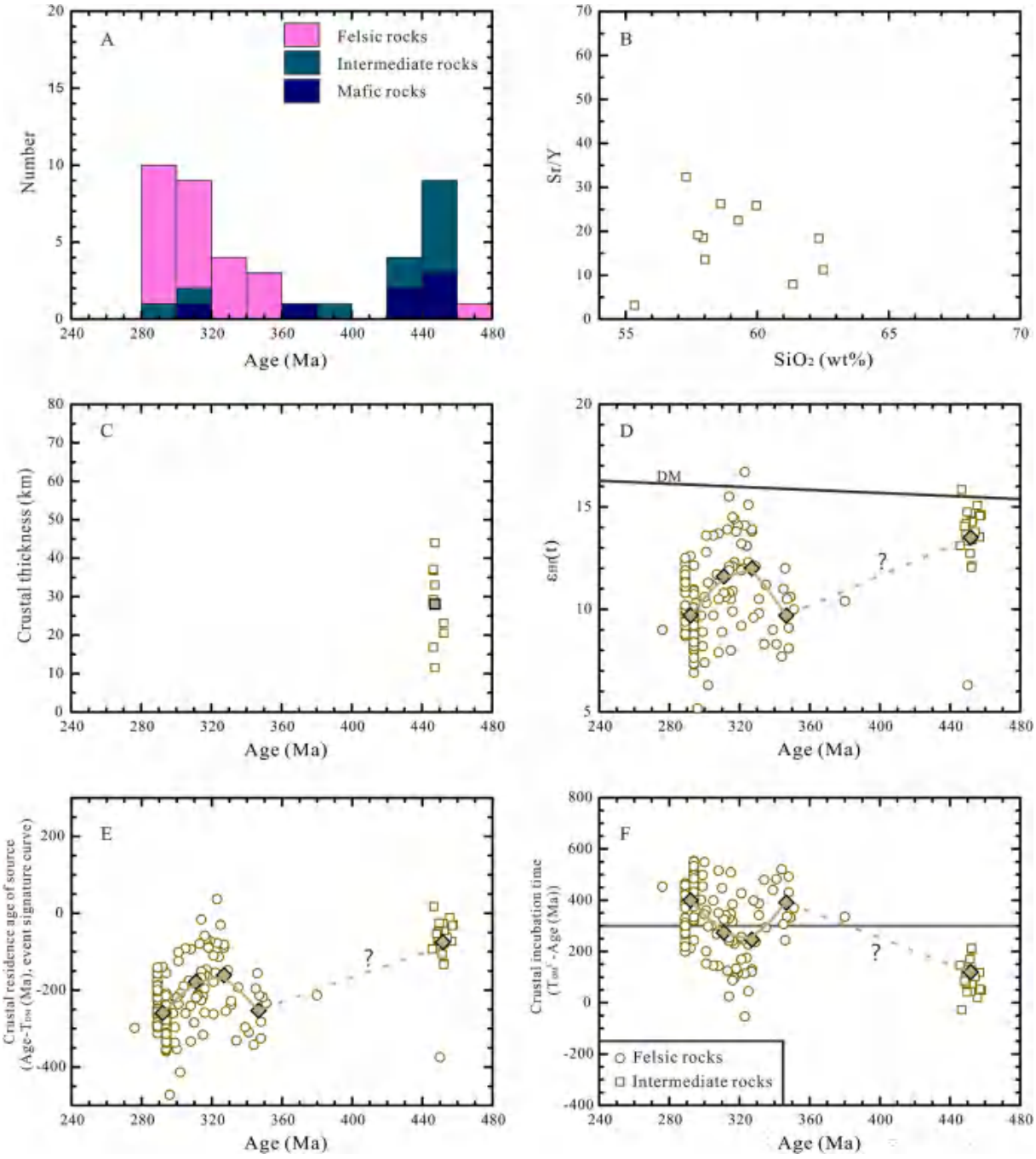


**Fig. 3.** Plots of (A) Histograms of compiled zircon U-Pb ages, (B) Sr/Y versus $SiO_2$ (wt%), (C) Crustal thickness versus zircon U-Pb ages, (D) $\varepsilon_{Hf}(t)$ versus zircon U-Pb ages, (E) Crustal residence age of source versus zircon U-Pb ages, and (F) Crustal incubation time versus zircon U-Pb ages classifications for Paleozoic igneous rocks from the Harlik belt in the Chinese Eastern Tianshan. The filled bold symbols are mean of the samples calculated every 20 million years. The lines between them represent their evolution over time.

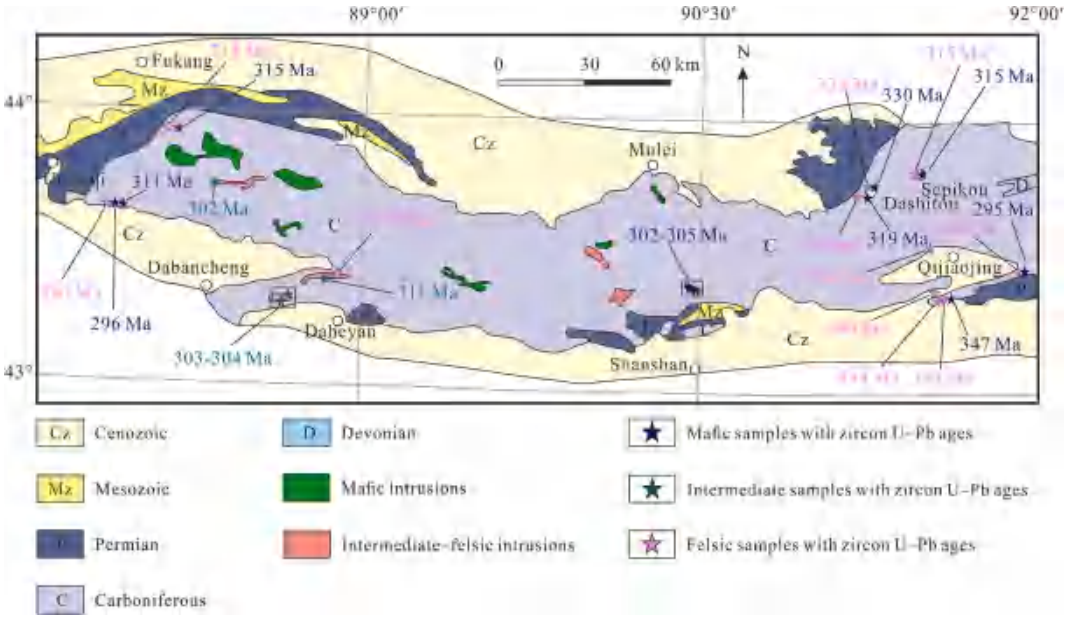


**Fig. 4.** Geological map of the Bogda belt (modified after Zhao et al., 2014 and Zhang et al., 2017). Detailed descriptions of the mafic–intermediate–felsic rocks can be found in Table S2.

Chen et al., 2013; Xie et al., 2016; Zhang et al., 2017). The Permian strata unconformably overlie the Carboniferous rocks and are composed of terrestrial conglomerate, sandstone, siliceous mudstone intercalated with bimodal volcanic lava (BGMRXUAR, 1993; Shu et al., 2011; Chen et al., 2013; Xie et al., 2016; Zhang et al., 2017).

The typical characteristics of magmatic activity in the Bogda area are multi-stage bimodal volcanic rocks (Figs. 4 and 5A; Table S2), such as ca. 345 Ma Hongshankou bimodal volcanism (Chen et al., 2013), ca. 330 Ma Dashitou bimodal volcanism (Zhang et al., 2017), and ca. 295 Ma bimodal volcanic rocks in the Baiyanggou, Qijiaojin, Hongshankou, and Cheguluquan areas (Chen et al., 2011).

### 2.3. The Dananhu belt

The Dananhu belt is located on the southern margin of the Turpan-Hami Basin and is a critical intra-oceanic island arc in the Eastern Tianshan (Figs. 1C and 6). In the Dananhu belt, the oldest sedimentary rocks are those of the Middle Ordovician Daliugou Group, which mainly consist of intermediate-felsic volcanic rocks inter-layered with basalts and radiolarian siliceous rocks, and intermediate-basic volcanic rocks inter-layered with felsic volcanic rocks (Tian et al., 2005). The Devonian strata unconformably overlie the Daliugou Group and are composed of mafic and pyroclastic rocks, clastic sediments, and calc-alkaline felsic volcanic lavas and tuffs, and the Carboniferous rocks mainly include lavas, pyroclastic rocks, greywacke, and carbonates (Xiao et al., 2004, 2013).

Paleozoic magmatic events took place at several episodes in the Dananhu belt (Figs. 6 and 7A; Table S3). It consists of Ordovician to Permian tholeiitic to calc-alkaline mafic–intermediate–felsic lavas, volcaniclastic rocks, sedimentary rocks (Zhang et al., 2018; Mao et al., 2022a, 2022b), abundant arc-related granitic intrusions (Du et al., 2018a, 2019a; Sun et al., 2019; Mao et al., 2022a), and the extensive Early Permian Alaska-type mafic–ultramafic complexes (Xiao et al., 2004; Han et al., 2010; Qin et al., 2011; Sun et al., 2019; Mao et al., 2022b). Recently, the Dacaotan ophiolite has been identified in central part of the Dacaotan area and zircon ages of ca. 417 Ma are obtained for the gabbros, and ca. 468 Ma and 463 Ma for the cumulate gabbros, respectively (She et al., 2017; Wang et al., 2022).

In addition, multiple types of mineral deposits of different ages have been documented in the Dananhu arc, including (1) VMS (volcanogenic massive sulfide) Cu-Zn-(Au/Ag) polymetallic deposits (Deng et al., 2016; Mao et al., 2022b); (2) porphyry Cu (Au/Mo) deposits associated with adakitic intrusions (Han et al., 2006; Mao et al., 2018; Gong et al., 2023); and (3) Cu-Ni sulfide deposits associated with the Early Permian mafic–ultramafic complex (Xiao et al., 2004; Han et al., 2010; Qin et al., 2011; Mao et al., 2022a).

### 2.4. The Kangguer belt

The Kangguer belt is a ca. 600 km long and 5 to 25 km wide accretionary complex, represents a suture zone that formed during the closure of the Kangguer Ocean (the east-extending of the North Tianshan Ocean) (Figs. 1C and 8; Xiao et al., 2004; Chen et al., 2019). This belt consists mainly of Devonian to Carboniferous volcano-sedimentary rocks and ophiolitic mélanges, and underwent intensive dextral strike-slip shearing deformation and greenschist facies metamorphism accompanied by localized thrusting during the Permian (Xiao et al., 2004; Wang et al., 2014).

The volcanic and sedimentary rocks of the Kangguer belt include sandstones, turbidites, lavas, and pyroclastic rocks (Xiao et al., 2004). These rocks are intensely deformed and metamorphosed, and converted to dark schists and meta-conglomerates (Zhang et al., 2014). Lower Permian volcanic rocks unconformably rest on the Carboniferous sequence in the Kangguer area, and Devonian volcanic rocks merely exposed in the north district of this belt (BGMRXUAR, 1993). The ophiolitic mélange of the Kangguer belt were formed in subduction-related environments based on the arc-like geochemical affinities of lavas, and mainly contain meta-basalt, meta-gabbro, chert, and serpentinized peridotite, with a Late Cambrian zircon U-Pb age (ca. 494 Ma) and an Early Carboniferous zircon U-Pb age (ca. 330 Ma) (Xiao et al., 2004; Li et al., 2008; Liu et al., 2016). In addition, based on the youngest zircons (ca. 317 Ma) obtained from turbiditic sandstones (Chen et al., 2019). The above evidence suggests that the existence of Kangguer Ocean prolonged at least from Cambrian to Carboniferous. Moreover, both subduction-related and post-collisional magmatic rocks have been identified in this belt (Figs. 8 and 9; Table S4; Wang et al., 2014; Du et al., 2019b).

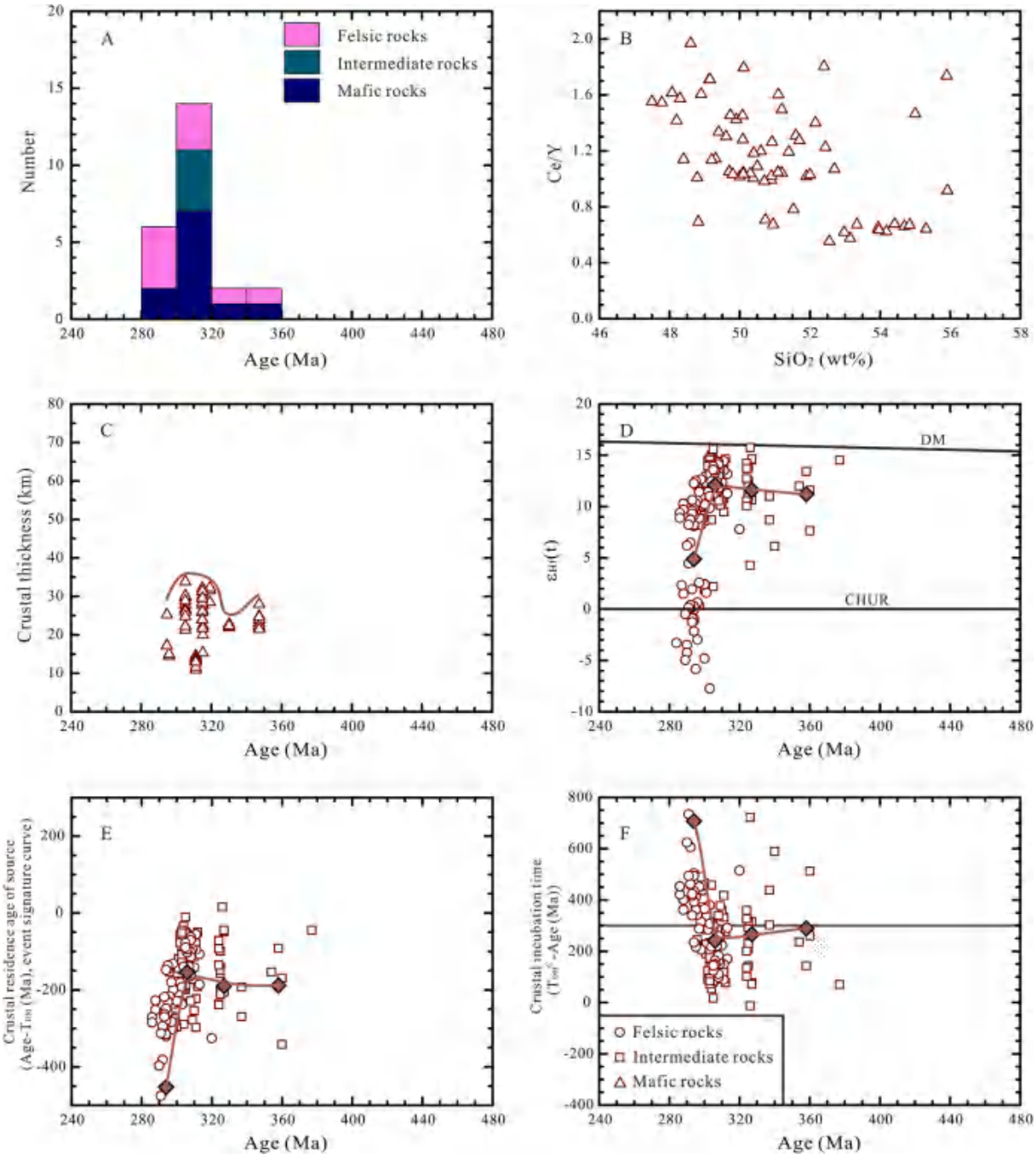


**Fig. 5.** Plots of (A) Histograms of compiled zircon U-Pb ages, (B) Ce/Y versus $SiO_2$ (wt%), (C) Crustal thickness versus zircon U-Pb ages, (D) $\varepsilon_{Hf}(t)$ versus zircon U-Pb ages, (E) Crustal residence age of source versus zircon U-Pb ages, and (F) Crustal incubation time versus zircon U-Pb ages classifications for Paleozoic igneous rocks from the Bogda belt in the Chinese Eastern Tianshan. The filled bold symbols are mean of the samples calculated every 20 million years. The lines between them represent their evolution over time.

### *2.5. The Yamansu belt*

The Yamansu belt is located in the north of the Central Tianshan Block and separated from it by the Aqikekuduke Fault (Fig. 1c). This belt is composed mainly of Carboniferous volcano-sedimentary rocks and Carboniferous to Triassic igneous intrusions (Figs. 10 and 11A; Table S5; Wu et al., 2006; Hou et al., 2014; Zhao et al., 2019a, 2019b). The Carboniferous volcanic rocks, including the Lower Carboniferous Yamansu and Gandun groups, and the Upper Carboniferous Tugutubulake, Wutongwozi and Qianshan groups, are characterized by bimodal volcanic rocks and interlayers of sedimentary rocks deposited in bathyal to shallow marine zones (Zhang et al., 2016; Long et al., 2020; Wu et al., 2022). Additionally, Permian volcanic and sedimentary rocks are distributed E–W and are scattered from north to south with a marine to continental sedimentary environment (Su et al., 2009; Long et al., 2020). The Carboniferous intrusions are widely developed and consist mainly of granite, granodiorite, and monzodiorite (Wu et al., 2006; Zhou et al., 2010; Du et al., 2018b; Zhao et al., 2019a, 2019b). The Permian intrusions are dominated by K-feldspar granite and granodiorite (Zhou et al., 2010; Du et al., 2018b; Zhao et al., 2019a, 2019b).

Furthermore, the Yamansu belt has been an important target for Fe exploration in NW China (Wang et al., 2006; Zhao et al., 2019a), with

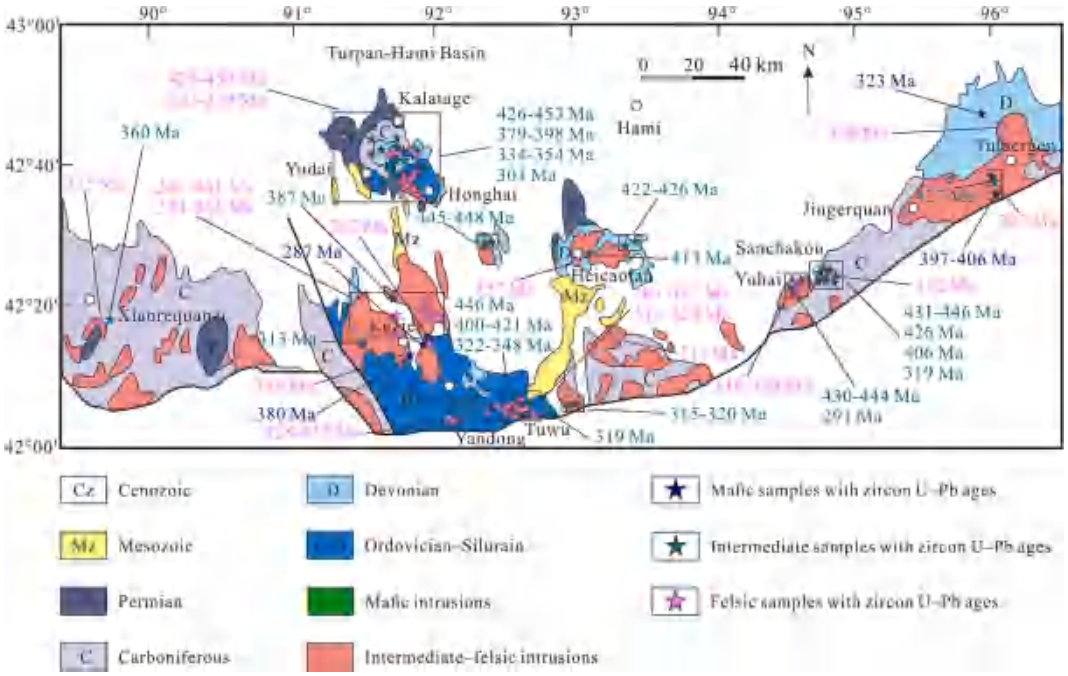


**Fig. 6.** Geological map of the Dananhu belt (modified after Sun et al., 2019 and Mao et al., 2022a). Detailed descriptions of the mafic–intermediate–felsic rocks can be found in Table S3.

many Fe (-Cu) deposits discovered, such as the Hongyuntan, Bailingshan, Duotoushan, Heijianshan, Chilongfeng, Yamansu, Heifengshan, Shuangfengshan and Shaquanzi deposits (Fig. 1C; Zhao et al., 2019a, 2019b).

### 2.6. The eastern part of the Central Tianshan

The eastern part of the Central Tianshan Block is a narrow domain separated from the Yamansu belt to the north by the Aqikekuduke Fault (Fig. 1C). It is characterized by a Proterozoic crystalline basement, including the Tianhu, Kawabulake and Xingxingxia groups, and most of them have experienced green-schist to amphibolite facies metamorphism and are unconformably overlain by or in fault contact with Paleozoic strata (Hu et al., 1998; Zhang et al., 2016). The basement is mainly composed of gneisses and migmatites overlain by Precambrian meta-sedimentary covers including clastic rocks, limestones and quartzites (1458–730 Ma) (Huang et al., 2015, 2017; Long and Huang, 2017). The basement rocks are overlain by widespread Ordovician volcanic rocks including calc-alkaline basalt, andesite, and pyroclastic rocks and Silurian sedimentary rocks, such as greywacke and metaflysch (Long et al., 2020). The volcanic rocks geochemically show calc-alkaline characteristics, and they were intruded by later granitoids (Dong et al., 2011; Lei et al., 2011). Based on studies on the basement, the Central Tianshan Block is usually considered as a part of the Tarim Craton during the Precambrian (Charvet et al., 2007, 2011; Ma et al., 2012). However, some researchers recently discovered that the source of Precambrian sediments in the Central Tianshan Block is different from that of the Tarim Craton and thus suggested a tectonic affinity not related to the Tarim Craton (He et al., 2015; Huang et al., 2015, 2017; Long and Huang, 2017).

## 3. Data compilation and application

Although the identification of advancing and retreating subduction zones is not always straightforward in a fossil accretionary orogen, previous studies in the West Pacifc, Andes, Cordillera and South China have shown that spatial-temporal trends with some unique fingerprints (e.g., magmatic rock composition, crustal thickness, isotopic excursions, and arc or trench migration) can be preserved in arc magmatic systems (DeCelles et al., 2009; Kemp et al., 2009; Chapman and Ducea, 2019; Spencer et al., 2019; Chen et al., 2020), possibly providing important information when attempting to distinguish the two types of subduction process. Advancing subduction is generally characterized by crustal shorting, thickening, and reworking in the overriding plate, and inboard migration of the arc or trench. In contrast, retreating subduction is marked by upper plate thinning, extension, splitting, crustal generation and oceanward migration of the magmatic arc (Cawood et al., 2009; Kemp et al., 2009).

In the present study, available data about the location, age (restricted to zircon U-Pb ages), lithology, major-trace elements, and zircon Hf isotope compositions of igneous rocks in the Eastern Tianshan are compiled and listed in Supplementary Tables S1, S2, S3, S4, and S5, in order to evaluate the variation of lithology distribution, crustal thickness, and crustal evolution trend over time in different tectonic zones.

### 3.1. Evaluate the spatial-temporal variations of magmatic rocks

It is known that systematic integration of the spatial-temporal variations for magmatic rocks in a given orogen is documented to be powerful in constraining their origin (e.g., Turner et al., 1999; Chung et al., 2005; Chen et al., 2020). Hence, the present study has compiled available data about the location, age, lithology, and geochemical compositions for the Paleozoic igneous rocks in the Eastern Tianshan.

Previous reports employed multiple geochronological techniques for estimating the timing of emplacement of the magmatic rocks, such as feldspar, biotite and/or hornblende Ar/Ar, zircon U-Pb and whole rock Rb-Sr. Zircon is physically and chemically resistant mineral and crystallizes relatively early during magma evolution, and its growth domains can commonly preserve the original information of magma crystallization. Therefore, here we compile zircon U-Pb ages (by LA-ICPMS, SHRIMP, TIMS, SIMS techniques) to represent timing of magmatism.

### 3.2. Crustal thickness estimation

Since trench advance and retreat commonly cause crustal thickening and thinning, respectively, tracing the changes in crustal thickness can

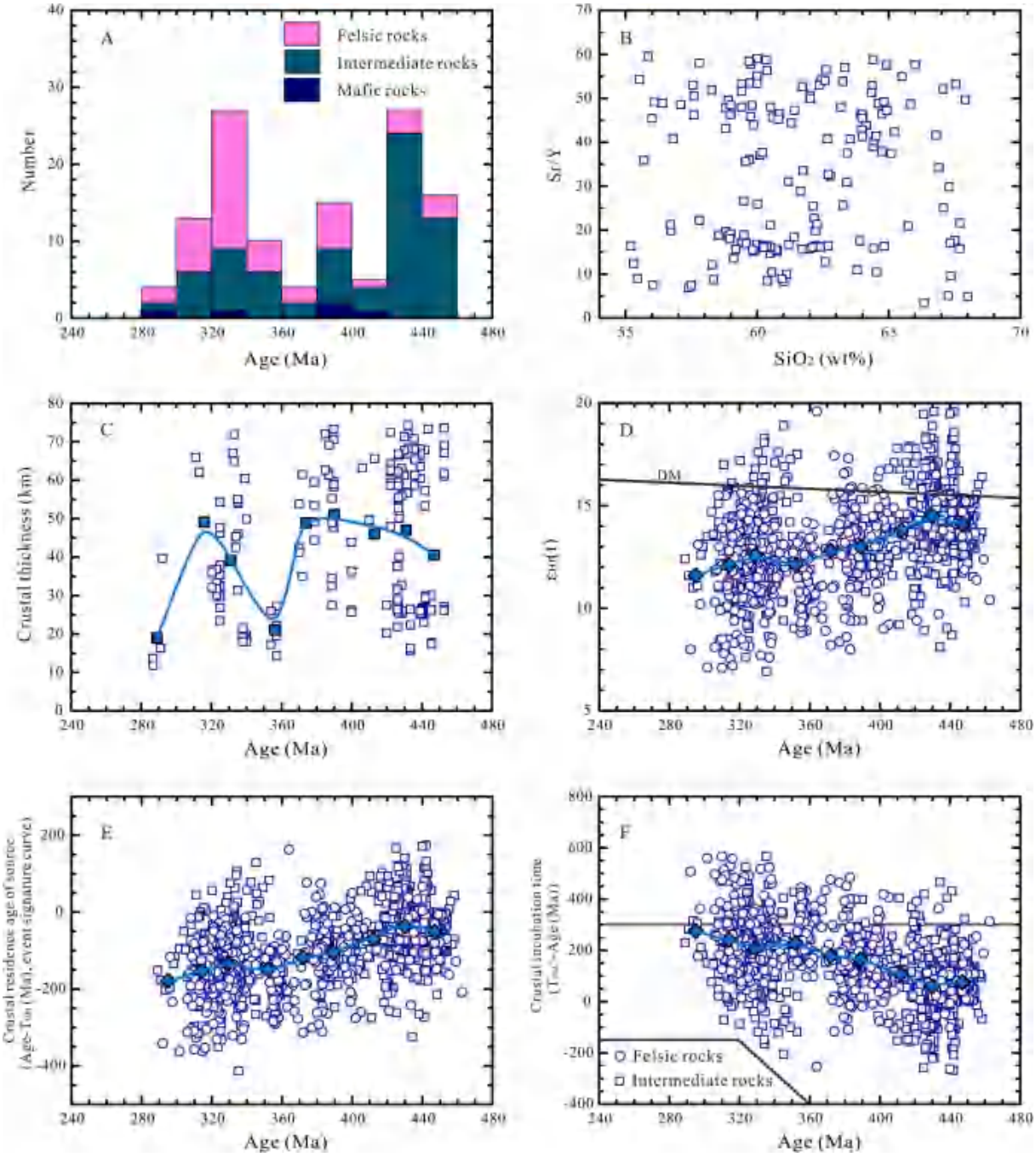


**Fig. 7.** Plots of (A) Histograms of compiled zircon U-Pb ages, (B) Sr/Y versus $SiO_2$ (wt%), (C) Crustal thickness versus zircon U-Pb ages, (D) $\varepsilon_{Hf}(t)$ versus zircon U-Pb ages, (E) Crustal residence age of source versus zircon U-Pb ages, and (F) Crustal incubation time versus zircon U-Pb ages classifications for Paleozoic igneous rocks from the Dananhu belt in the Chinese Eastern Tianshan. The filled bold symbols are mean of the samples calculated every 20 million years. The lines between them represent their evolution over time.

provide crucial clues to refine the subduction-accretion process (Zhang et al., 2018; Wang et al., 2022; Gong et al., 2023). Several studies have successfully investigated the application of geochemical proxies to estimate crustal thickness in subduction and collisional settings, such as Ce/Y of basaltic rocks and Sr/Y, La/Yb, Dy/Yb, and Ho/Yb of crust-derived intermediate and felsic rocks, all of which are sensitive to the absence or presence of plagioclase (or garnet) in magma genesis and increase with increasing crustal depths (Mantle and Collins, 2008; Chapman et al., 2015; Profeta et al., 2015; Hu et al., 2017; Zhang et al., 2018; Wang et al., 2022; Gong et al., 2023).

During partial melting of lower crustal igneous rocks such as gabbros and their metamorphic equivalents or during magmatic fractionation of mantle-derived mafic magmas, Sr is compatible at low pressures (<~1.0 Gpa) where it strongly partitions into plagioclase (Chapman et al., 2015; Profeta et al., 2015). However, at high pressures (>1.2 Gpa), where plagioclase is unstable, Sr is incompatible and preferentially enters the liquid phase (Chapman et al., 2015; Profeta et al., 2015). Conversely, Y is incompatible at low pressures, but readily partitions into garnet and amphibole at high pressure (e.g., Lee et al., 2007). As a result, Sr/Y is a common qualitative indicator of the average crustal pressure, or depth, at which magmatic differentiation occurred, and the variability in Sr/Y for intermediate compositions when averaged over multiple arcs has

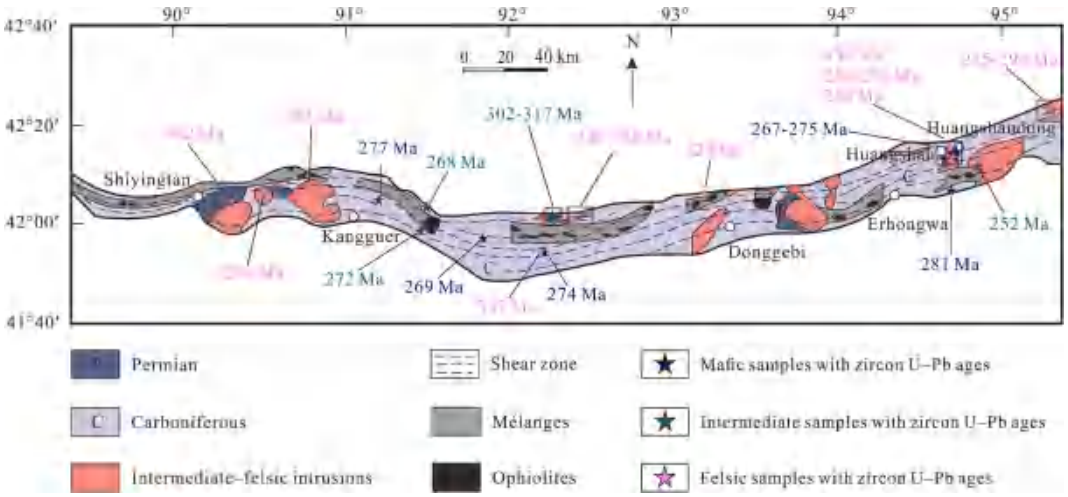


**Fig. 8.** Geological map of the Kangguer belt (modified after Zhao et al., 2019b and Mao et al., 2022c). Detailed descriptions of the mafic–intermediate–felsic rocks can be found in Table S4.

recently been correlated to crustal thickness globally (Chapman et al., 2015; Profeta et al., 2015).

The Eastern Tianshan terrane experienced subduction and accretion processes and ultimately a collisional phase during Paleozoic (Xiao et al., 2004; Zhang et al., 2018; Wang et al., 2022). Almost all data in this study overlap well with those in rocks from subduction-related arcs rather than from continental collisional belts (Profeta et al., 2015; Hu et al., 2017; Wang et al., 2022). Finally, we preferentially employ the Sr/Y ratios of intermediate rocks to monitor the crustal thickness following Profeta's method throughout the Paleozoic time (Profeta et al., 2015; Wang et al., 2022). To better monitor the crustal thickness, the data was filtered to include rocks with $SiO_2$ (55–68 wt%), MgO (0.5–4 wt%), and Rb/Sr (<0.2) content to eliminate mafic rocks that were possibly derived from the mantle and highly fractionated granites (Chapman et al., 2015; Profeta et al., 2015; Wang et al., 2022). On the other hand, due to altered mid-ocean ridge basalts have higher Sr than basalts/gabbros from sub arc environments, Sr/Y ratio of the magma generated by slab melting is >60 (Defant and Drummond, 1990; Profeta et al., 2015). Hence, data with high Sr/Y ratios (>60) were also discarded because they were probably generated by slab melting (Defant and Drummond, 1990; Profeta et al., 2015).

Moreover, considering that few geochemical analyses for intermediate rocks were reported in the Bogda back-arc basin (Table S2). As an alternative, the maximum Ce/Y ratios of basaltic rocks can constrain the minimum melting depth and crustal thickness (Mantle and Collins, 2008), thus we utilize the Ce/Y ratios of basaltic rocks to measure the crustal thickness of the Bogda belt.

### 3.3. Crustal evolution trend estimation

The amount of juvenile continental crust generated in the CAOB is highly variable (~64% to ~14%; Jahn et al., 2000, 2004; Kröner et al., 2014, 2017; Yang et al., 2017; Wang et al., 2022, 2023). The anomalously high proportion of juvenile component in the granitoids (Jahn et al., 2000, 2004) of the CAOB was attributed to the incorporation of anorogenic intraplate magmatism and/or a lack of consideration of the role of crustal reworking in the magma sources (Kröner et al., 2014, 2017). Hence, the key is to figure out the relative roles of crustal growth and crustal reworking, and further thoroughly understand whether there is a link between the crustal architecture and subduction pattern (advancing/retreating subduction) (Armstrong, 1981; Belousova et al., 2009; Dhuime et al., 2012; Kröner et al., 2014; Tang et al., 2017; Wang et al., 2023).

Zircon is a common accessory mineral in granitoid rocks, and its Lu-Hf isotopic composition is a powerful tool in tracing the nature of crustal rocks and determining the evolutionary history of crust (Griffin et al., 2004; Kemp et al., 2006). In general, magmatic rocks derived wholly from the depleted mantle exhibit highly positive zircon $\varepsilon_{Hf}(t)$ values, whereas magmatic rocks generated entirely by the reworking of ancient continental crust show negative zircon $\varepsilon_{Hf}(t)$ values, and magmatic rocks formed by magma mixing display large variations in $\varepsilon_{Hf}(t)$ values (Griffin et al., 2004; Kemp et al., 2006). However, the granitoid rocks that formed by the reworking of juvenile crust from those that directly originated from mantle, which both have positive zircon $\varepsilon_{Hf}(t)$ values.

Single-stage Hf model age ($T_{DM}$) was calculated based on a depleted-mantle source, can give a minimum age for the source material of the magma from which the zircon crystallized (Griffin et al., 2006; Belousova et al., 2009). The U-Pb ages plotted against the difference between zircon U-Pb ages and Hf model ages (Age–$T_{DM}$) can be simplified to "event signature curves", in which illustrated the evolutionary features of crustal residence age of magma source (Griffin et al., 2006; Belousova et al., 2009). These researchers proposed an increasing trend with decreasing age indicates addition of juvenile materials and a downward trend with decreasing age reflects ancient crustal reworking, while magma mixing between them produces an intermediate slope (Griffin et al., 2006; Belousova et al., 2009). In addition, reworking of ancient crust will create a downward trend with decreasing age and negative $\varepsilon_{Hf}(t)$ values, while reworking of juvenile crust will generate a downward trend with decreasing age as well as positive but relatively low $\varepsilon_{Hf}(t)$ values (Du et al., 2021).

As most zircons having crystallized from quartz-saturated magma were produced by partial melting of the crust through two steps: Hf crustal model ages define the step 1, separation of primitive crust from the mantle; and U-Pb ages date the step 2, widespread melts of the primitive crust to form granitoids (Wang et al., 2009, 2011). Therefore, "Crustal incubation time" is another crucial indicator in revealing the crustal evolution, which is defined as the difference between the Hf crustal model age and zircon U-Pb age ($T_{DM}^{C}$–Age) (Wang et al., 2009, 2011; Li et al., 2014). The zircons generated by juvenile crustal materials have crustal incubation time <300 Ma (Wang et al., 2009, 2011), whereas the zircons formed by the reworking of pre-existing ancient crust will result in high crustal incubation times (>300 Ma) (Wang et al., 2009, 2011; Li et al., 2014; Huang et al., 2019). Hence, we also regarded crustal incubation time of 300 Ma as the dividing line between the juvenile crust and ancient crust in this study, and assumed that short crustal incubation time (<300 Ma) generally reflects a juvenile material addition, whereas long crustal incubation time (>300 Ma) indicates an ancient crust reworking (Wang et al., 2009, 2011; Li et al., 2014; Huang

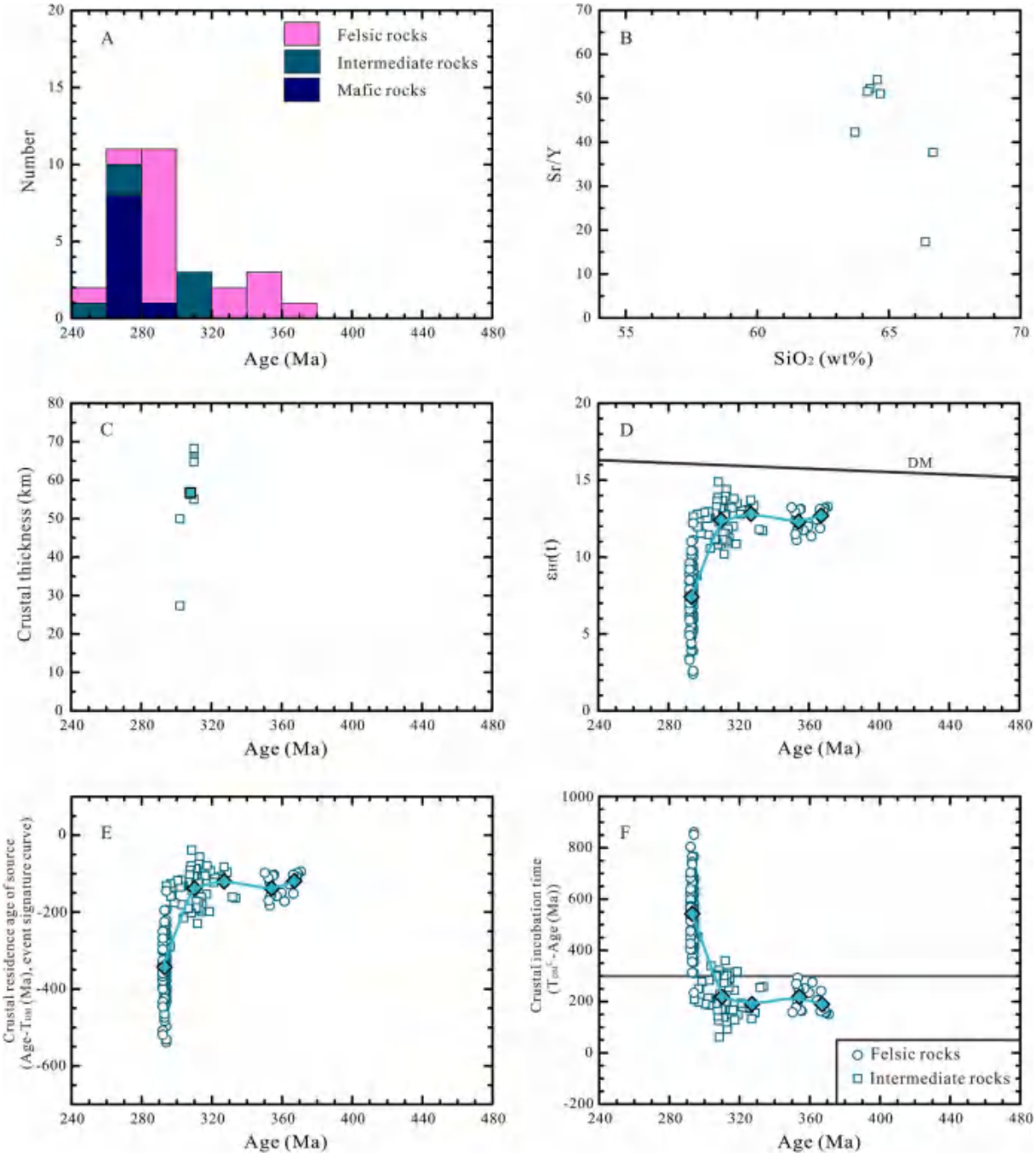


**Fig. 9.** Plots of (A) Histograms of compiled zircon U-Pb ages, (B) Sr/Y versus $SiO_2$ (wt%), (C) Crustal thickness versus zircon U-Pb ages, (D) $\varepsilon_{Hf}(t)$ versus zircon U-Pb ages, (E) Crustal residence age of source versus zircon U-Pb ages, and (F) Crustal incubation time versus zircon U-Pb ages classifications for Paleozoic igneous rocks from the Kangguer belt in the Chinese Eastern Tianshan. The filled bold symbols are mean of the samples calculated every 20 million years. The lines between them represent their evolution over time.

et al., 2019).

Although a specific tectonic setting does not necessarily produce magmas with unique Hf isotopic composition of zircons, long-term Hf-in-zircon variations have succeeded in revealing the relative contribution of juvenile and ancient crustal components as well as discriminating the trench advance and retreat in accretionary orogens (e.g., Boekhout et al., 2013; Collins et al., 2011; Zhang et al., 2019; Wang et al., 2023). Collectively, in order to identify the Paleozoic evolutionary characteristics of the Eastern Tianshan, we comprehensive analysis the zircon $\varepsilon_{Hf}(t)$ values, event signature curves, and crustal incubation time of the Paleozoic granitoids ($SiO_2$ > 55 wt%) in the Eastern Tianshan.

## 4. Patterns for spatial-temporal variations in lithology composition

### 4.1. The Harlik belt

The Harlik Early Paleozoic volcanic rocks were originally assigned to the Middle–Late Ordovician (BGMRXUAR, 1993). Recently, Zhao et al. (2022) proposed that the volcanic rocks overlie the Middle–Late Ordovician sediments with an angular unconformity in the Harlik terrane. Zircon U-Pb dating of these volcanic rocks, i.e., ca. 441 Ma of the tholeiitic basalts, 440 Ma of the tuffs, and 434 Ma of the alkaline basalts,

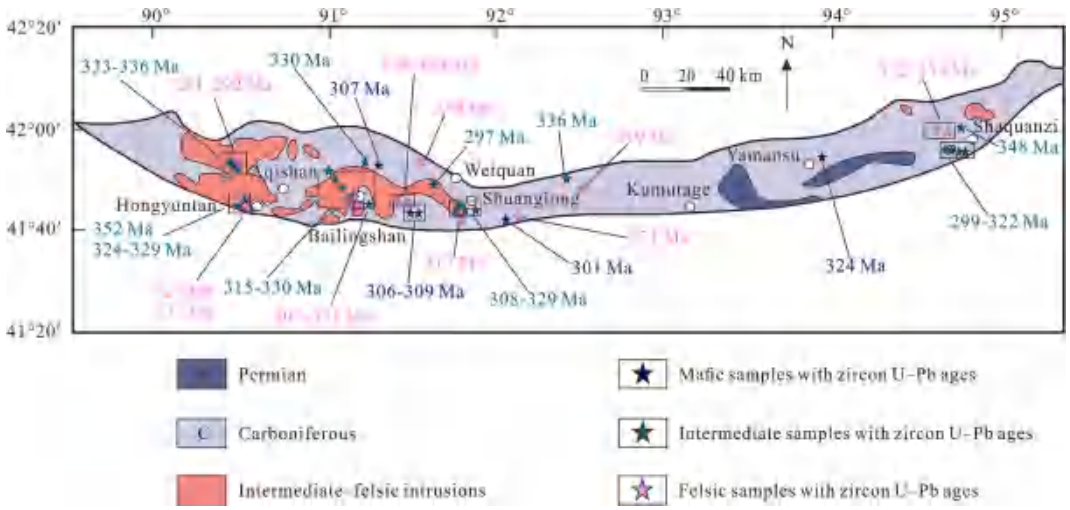


**Fig. 10.** Geological map of the Yamansu belt (modified after Zhang et al., 2016 and Zhao et al., 2019b). Detailed descriptions of the mafic–intermediate–felsic rocks can be found in Table S5.

indicate that the volcanic rocks in the Harlik terrane erupted in the Early Silurian (Fig. 2; Table S1; Zhao et al., 2022). On the other hand, various ages have recently been accepted for the Early Paleozoic intrusive rocks (Figs. 2 and 3A; Table S1; e.g., Cao et al., 2006; Guo et al., 2006; Ma et al., 2015; Du et al., 2018a). The arc-like geochemical features of these Early Paleozoic igneous rocks demonstrate they were both generated in an arc-related tectonic setting (e.g., Deng et al., 2016; Du et al., 2018a; Zhang et al., 2019). Thus, based on the combined data from previous investigations, the onset of arc magmatism in the Harlik belt was during Middle Ordovician to Late Silurian (Xiao et al., 2004; Zhang et al., 2018; Du et al., 2021; Mao et al., 2022a).

Then, there is a long magmatic interval from ca. 420 Ma to 360 Ma in the Harlik belt and only few igneous rocks formed at this interval have geochemical data, consistent with the zircon age spectra of detrital zircons in the Carboniferous sandstones (Fig. 3A; Huang et al., 2018). Alternatively, the 360–280 Ma suite of granitoids is widely distributed in this belt, accompanied by a small amount of intermediate–mafic rocks (Figs. 2 and 3A). Predictably, previous studies in the Harlik arc have mainly focused on the Late Paleozoic tectonic evolution and related granitoids (e.g., Yuan et al., 2010; Ma et al., 2015; Du et al., 2018a). In particular, some extension-related magmatic activities have been reported during this period, such as Carboniferous to Early Permian A-type granites in the Xiaobaiyanggou, Qincheng, Xiamaya, Shichengzi areas, etc. (e.g., Yuan et al., 2010; Huang, 2014; Chen et al., 2016; Wang et al., 2016).

### 4.2. The Bogda belt

This belt, located between the Dananhu and the Harlik arcs, has been regarded as an Early Carboniferous back-arc basin and consists mainly of Carboniferous and Permian strata (Fig. 4; Chen et al., 2013; Zhang et al., 2017). Previous geochronological and geochemical studies have revealed that multi-phase of bimodal volcanism occurred in the Bogda belt. However, the magmatism was largely restricted to the Carboniferous to Early Permian (Figs. 4 and 5A; Table S2), including (1) ca. 345 Ma Heishankou bimodal volcanism (Chen et al., 2013), (2) ca. 330 Ma Dashitou bimodal volcanism (Zhang et al., 2017), (3) ca. 315 Ma Sepikou bimodal volcanism (Gao et al., 2013), and (4) ca. 295 Ma Qijiaojing bimodal volcanism (Chen et al., 2011). In contrast, intermediate rocks are rarely reported (Figs. 4 and 5A; Table S2).

### 4.3. The Dananhu belt

Decades of researches have shown that the Dananhu arc in the Eastern Tianshan orogen is mainly an intra-oceanic arc that was generated by subduction of the Kangguer Ocean, an important branch of the Paleo-Asian Ocean (Xiao et al., 2004; Zhang et al., 2018; Mao et al., 2022a, 2022b, 2022c). It experienced long-lively complicated subduction accretionary processes from the Ordovician to the Permian, and has discontinuous polyphase generations and types of igneous rocks (Xiao et al., 2004; Du et al., 2018a, 2019a; Zhang et al., 2018; Sun et al., 2019; Mao et al., 2022a, 2022b, 2022c). In particular, the earliest strata in the Dananhu belt predominantly consists of pyroclastic and volcanic rocks deposited in the Middle Ordovician to Devonian (BGMRXUAR, 1993; Xiao et al., 2004).

The onset of arc magmatism in the Dananhu arc was considered between Middle Ordovician and Late Silurian, such as ca. 460–420 Ma gabbro diorites, diorites, granites, and high-MgO andesites (Figs. 6 and 7A; Table S3; Du et al., 2018a; Zhang et al., 2018; Sun et al., 2019; Zhang et al., 2022; Zhao et al., 2022). As shown in Table S3 and illustrated in Figs. 6 and 7A, in comparison with the widespread occurrence of the earlier and later rocks, the Devonian magmatic rocks emplaced within a restricted number of distributions without obvious magmatism quiescence. The magmatic rocks emplaced at 420–360 Ma appear to be limited to the southernmost part of the Dananhu belt, and are mainly diorites and granites (Du et al., 2018a, 2019a; Zhang et al., 2018; Sun et al., 2019; Mao et al., 2022a, 2022b). The 360–300 Ma suite of rocks are widely distributed throughout the Dananhu arc, and are also dominated by intermediate to felsic rocks (Du et al., 2018a, 2019a; Zhang et al., 2018; Sun et al., 2019; Mao et al., 2022a, 2022b). Based on Sr/Y and Y values, the Carboniferous granitoids can be subdivided into two types: the adakitic granites and normal granites (Du et al., 2019a). Rocks belonging to the 300–280 Ma suite only crop out in the Sha'erhu, Kalatage, and Yuhai-Sanchakou areas (Mao et al., 2014, 2022a; Wang et al., 2018). In addition, extensional structures and magmatism were represented by the Late Devonian (ca. 380–357 Ma) high-Al gabbros and A-type granites in the Kezi'er area, and Early Permian (ca. 287) alkaline gabbro and A-type rhyolites in the Sha'erhu area (Mao et al., 2014, 2022a; Du et al., 2023).

### 4.4. The Kangguer belt

The Kangguer belt represents the suture zone of the northern Tianshan Ocean, which is a southern branch of the Paleo-Asian Ocean remnants (Xiao et al., 2004; Li et al., 2008; Chen et al., 2019; Ao et al., 2021). The Kangguer Ocean was a long-lived Ocean existed at least from ca. 494 to ca. 317 Ma (Li et al., 2008; Chen et al., 2019). However, the Kangguer belt lacks pre-Devonian magmatic activity. The Devonian

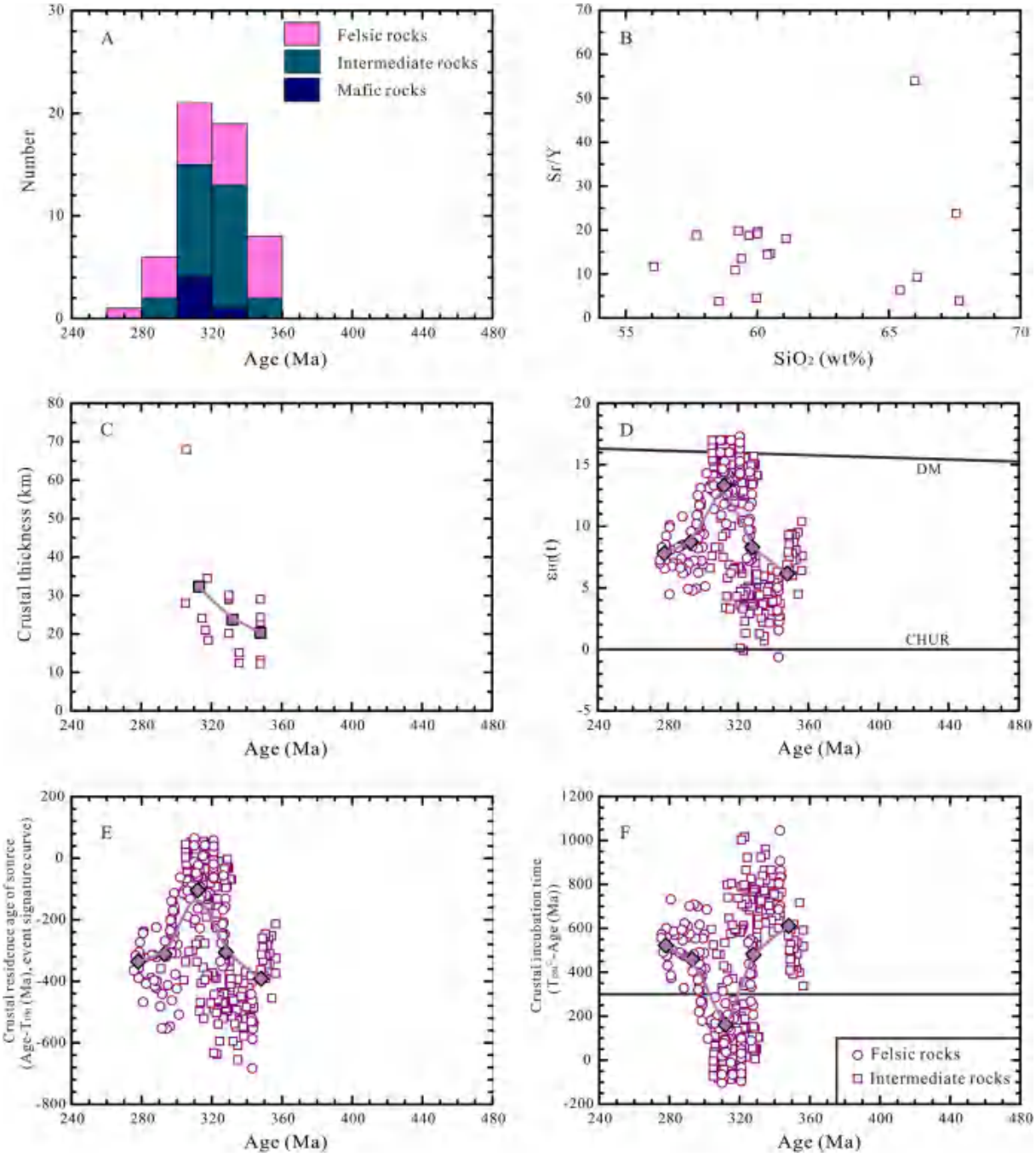


**Fig. 11.** Plots of (A) Histograms of compiled zircon U-Pb ages, (B) Sr/Y versus $SiO_2$ (wt%), (C) Crustal thickness versus zircon U-Pb ages, (D) $\varepsilon_{Hf}(t)$ versus zircon U-Pb ages, (E) Crustal residence age of source versus zircon U-Pb ages, and (F) Crustal incubation time versus zircon U-Pb ages classifications for Paleozoic igneous rocks from the Yamansu belt in the Chinese Eastern Tianshan. The filled bold symbols are mean of the samples calculated every 20 million years. The lines between them represent their evolution over time.

volcanic sedimentary rocks only occur to the north of the shear zone and consist of basalt and andesite with minor rhyolite, dacite, volcanic breccia, tuff and clastic rocks, but lack chronological evidence (BGMRXUAR, 1993). Available geological maps and previous studies suggest that the granitoids in the Eastern Tianshan are associated with volcanic and volcano-sedimentary rocks (BGMRXUAR, 1993). Recently, a Late Devonian age (360 ± 3 Ma) was obtained from a porphyritic granitic intrusion along the northern edge of the Kangguer belt (Du et al., 2019b).

This belt is mainly comprised of Carboniferous volcaniclastic rocks that have been metamorphosed to greenschist facies, and associated with abundant granites (Xiao et al., 2004; Wang et al., 2014). In contrast, the Permian magmatic rocks are widely distributed throughout the belt, various from felsic to mafic–ultramafic intrusions, including the Huangshan, Baishiquan, and Baishan intrusions, etc. (Figs. 8 and 9A; Table S4; Zhou et al., 2010; Wang et al., 2014; Cao et al., 2017; Du et al., 2019b). There are also gold deposits in the west of the zone (e.g., Shiyingtan and Kangguer; Rui et al., 2002; Zhang et al., 2002) and ca. 300–270 Ma Cu-Ni deposits in the east (e.g., Huangshan and Huangshandong; Xiao et al., 2010; Pirajno et al., 2011; Qin et al., 2011; Su et al., 2011; Deng et al., 2015).

### 4.5. The Yamansu belt

The Yamansu belt is located at the northern margin of the Central Tianshan Block and is composed mainly of Carboniferous arc-related volcanic rocks and Carboniferous to Triassic intrusions (Wu et al., 2006; Hou et al., 2014). The Early Carboniferous arc-related magmatic rocks appear to be limited to the west part of this belt, including calc-alkaline volcanic rocks series (basalt, andesite, and dacite) from the Yamansu group with zircon U-Pb ages of 348 to 324 Ma (Luo et al., 2012, 2016; Hou et al., 2014; Wu et al., 2022), and the intermediate to felsic intrusions of the Aqishan mountain, Xifengshan, Shiyingtan, and Changtiaoshan area show similar U-Pb ages of 349 to 323 Ma (Wu et al., 2006; Zhou et al., 2010; Du et al., 2018b; Long et al., 2020).

In contrast, the Late Carboniferous (ca. 322–302 Ma) magmatic rocks are widely distributed throughout the Yamansu belt, and some representatives include ca. 320 Ma MORB-like volcanic rocks from the Wutongwozi Formations and ca. 318–307 Ma calc-alkaline granites from the Bailinshan pluton (Figs. 10 and 11A; Table S5; Zhou et al., 2010; Luo et al., 2016; Zhang et al., 2016). In comparison with the widespread occurrence of Late Carboniferous rocks, magmas emplaced at 301–270 Ma appear to be limited (Du et al., 2018b; Zhao et al., 2019a, 2019b; Zhang et al., 2020). These include some extensional magmatism, for instance, the Dikan'er Nb-rich basalts and Aqishan mountain A-type granites (Du et al., 2018b; Zhang et al., 2020).

## 5. Patterns for spatial-temporal variations in crustal thickness

### 5.1. The Harlik belt

Crustal thickness calculated by median Sr/Y ratio of intermediate rocks of the Harlik belt are plotted against age in Fig. 3B, but there were only few geochemical analyses for intermediate rocks or other types rocks reported in the Harlik arc (Table S1). Limited geochemical data of the Late Ordovician intermediate rocks suggest that the crustal thickness varies from 11.7 to 44.1 km during this period, with an average crustal thickness of 28.2 km (Fig. 3C), which represents the initial stage of development of the Harlik arc crust.

### 5.2. The Bogda belt

Considering the lack of geochemical analyses reported for intermediate rocks in the Bogda back-arc basin, we tend to employ the maximum Ce/Y ratios of basaltic rocks to monitor the minimum melting depth and crustal thickness of the Bogda belt, due to the greatest variability in the Sr/Y ratios for arc thicknesses of 25–30 km occurs similar to the largest variability in the Ce/Y ratios for arc thicknesses of ~30 km (Table S2; Chapman et al., 2015; Mantle and Collins, 2008). In addition, the mafic rocks in the Bogda belt do not exhibit obvious correlations between Ce/Y and $SiO_2$, arguing against significant crystallization effect on the variable of Ce/Y ratios (Fig. 5B). The Ce/Y ratios could therefore provide constraints on the variation of crustal thickness in the Bogda Belt (Fig. 5C).

The Bogda belt displays repeated crustal thinning and thickening during the restricted time (ca. 347–295 Ma) (Fig. 5C). Based on the changes in maximum Ce/Y ratios of mafic rocks, the calculated crustal thickness was 28.0 km at ca. 347 Ma, 22.8 km at ca. 330 Ma, 33.8 km during ca. 319–305 Ma, and 25.3 km during ca. 296–295 Ma (Fig. 5C). The Ce/Y data compiled here suggest that the Bogda crustal thickness went through two significant pulsed of thinning, one during the Early Carboniferous (ca. 347–330 Ma), and the other during the Early Permian (ca. 296–295 Ma), separated by periods of crustal thickening during ca. 319–305 Ma (Fig. 5C).

### 5.3. The Dananhu belt

In comparison with other tectonic units in the Eastern Tianshan with limited rocks types or time, the Paleozoic mafic to felsic magmatic rocks are widely distributed throughout the Dananhu belt (Figs. 6 and 7A; Table S3). The intermediate rocks in the Dananhu belt do not exhibit obvious correlations between Sr/Y and $SiO_2$ (Fig. 7B), we preferentially employ the Sr/Y ratios of intermediate rocks to monitor the crustal thickness of the Dananhu belt following Profeta's method throughout the Paleozoic time (Fig. 7C; Profeta et al., 2015; Wang et al., 2022).

The Dananhu belt displays cyclical crustal thickening and thinning during the Paleozoic time, with two significant pulses of crustal thickening, one during the Late Ordovician to Late Devonian (ca. 460–381 Ma), and the other during the Early Carboniferous (ca. 360–321 Ma). Correspondingly, two episodes of crustal thinning occur within the two pulses of crustal thickening, one during ca. 380–361 Ma, and the other during ca. 320–280 Ma) (Fig. 7C). Crustal thickness calculated by median Sr/Y ratio of intermediate rocks of the Dananhu belt suggest that the average crustal thickness for the initial stage of development of the Dananhu arc crust was 40.5 km, the timing of the two maximum crust thickness (51.1 km and 49.1 km) was at ca. 390 Ma and ca. 316 Ma, and the two periods of the thinnest crust (21.1 km and 19.0 km) were at ca. 356 Ma and ca. 289 Ma (Fig. 7C and Table S3).

### 5.4. The Kangguer belt

Similar to the Harlik belt, there were few geochemical analyses of intermediate rocks or mafic rocks reported in the Kangguer belt (Figs. 8 and 9B; Table S4). The available geochemical data from the Late Carboniferous intermediate rocks suggest that the crustal thickness various from 27.3 to 68.3 km during ca. 310 to ca. 302 Ma, with an average crustal thickness of 56.7 km (Fig. 9C and Table S4).

### 5.5. The Yamansu belt

As shown in Fig. 11B, the intermediate rocks in the Yamansu belt do not show significant correlations between Sr/Y ratios and $SiO_2$, thus the Sr/Y ratio was employed as a proxy to monitor the crustal thickness of the Yamansu belt (Chapman et al., 2015; Profeta et al., 2015; Wang et al., 2022). The average crustal thickness in the earliest magmatic episode (ca. 348 Ma) of the Yamansu belt was about 20.3 km. Subsequently, the Yamansu crustal thickening changed during the Carboniferous and culminated with median 32.3 km thick crust at ca. 318–305 Ma (Fig. 11C and Table S5). Nevertheless, variations in crustal thickness of the Yamansu belt after Carboniferous have not been observed.

## 6. Patterns for spatial-temporal variations in crustal evolution trend

### 6.1. The Harlik belt

There were more zircon geochemical data for the intermediate-felsic rocks than the whole-rock geochemical analyses of intermediate rocks in the Harlik arc, and the zircon $\varepsilon_{Hf}(t)$ patterns with Hf model ages may be related to the evolution of the crust in which they occur (Griffin et al., 2006; Belousova et al., 2009; Wang et al., 2009, 2011; Li et al., 2014; Huang et al., 2019). The Late Ordovician granitoids in the Harlik belt were characterized by highly positive zircon $\varepsilon_{Hf}(t)$ values, in particular, low crustal incubation time are consistent with the presence of depleted mantle material (Fig. 3D-F). After the long magmatic silence of the Harlik belt from ca. 420 Ma to 360 Ma, the zircon $\varepsilon_{Hf}(t)$ value at ca. 350 Ma is still positive, but it is significantly lower than the initial stage of this belt (Fig. 3D). Accordingly, the magmatic zircons have a long crustal incubation time during this period. Then, the intermediate-felsic rocks of the Harlik segment exhibit trends of increasing zircon $\varepsilon_{Hf}(t)$ values with decreasing age before ca. 330 Ma and then decreasing zircon $\varepsilon_{Hf}(t)$ subsequently, consistent with shifts to sharp rising trend of event signature curve with decreasing crustal incubation time before 330 Ma, and then to downward trend with decreasing age of the event signature

curve in addition to show increasing crustal incubation time thereafter (Fig. 3D-F). Zircon $\varepsilon_{Hf}(t)$ value tends to be increasing with decreasing age and event signature curve to be increasing in the samples of the Harlik belt with shorter crustal incubation time, implying that these rocks are associated with crustal evolution.

### 6.2. The Bogda belt

As stated in the section 4.2, the Bogda belt is characterized by multiple stages of bimodal volcanic rocks. Recently, Zhang et al. (2020, 2021) also found some intermediate rocks in the Daheyan and Tonggou areas, and in particular, obtained some zircon Hf isotope data (Table S2). Combined with the previously reported zircon Hf data of rhyolites imply that zircon $\varepsilon_{Hf}(t)$ values of the intermediate-felsic rocks slowly rising started during the Late Devonian to Late Carboniferous (ca. 370–300 Ma) and culminated with mean of 12.1 at ca. 306 Ma (Fig. 5D and Table S2). Meanwhile, samples show slowly rising trend of zircon $\varepsilon_{Hf}(t)$ values with decreasing emplacement age also to exhibit sluggish rising trend of event signature curve with time and to have low crustal incubation time (Fig. 5D-F).

Subsequently, from latest Carboniferous to Early Permian (ca. 300–284 Ma), the zircons from the Bogda samples show large variations in $\varepsilon_{Hf}(t)$ values and have wide range of crustal residence ages as well as crustal incubation time (Fig. 5D-F). Compared to rocks before ca. 300 Ma, they show gradually decrease of the average $\varepsilon_{Hf}(t)$ values, and display a remarkable downward trend with decreasing age of the event signature curve in addition to have long crustal incubation time (Fig. 5D-F).

### 6.3. The Dananhu belt

The Hf isotopic characteristics of the intermediate and felsic rocks in the Dananhu belt exhibit broadly similar patterns in rocks of different ages (Fig. 7D-F). The first magmatic episode (ca. 460–440 Ma) rocks in the Dananhu belt were characterized by highly positive $\varepsilon_{Hf}(t)$ values, but low crustal incubation time, which is similar to the samples of the Harlik arc at the same time (Figs. 3 and 7). From Late Ordovician to Late Silurian (ca. 460–420 Ma), zircons from the Dananhu belt granitoids maintain highly positive $\varepsilon_{Hf}(t)$ values and show sharp rising trend of event signature curve, in addition to most of the magmatic zircons have a short crustal incubation time (Fig. 7D-F).

Following the brief rising trend of the $\varepsilon_{Hf}(t)$ values, then, from Late Silurian to Late Devonian (ca. 420–360 Ma), the zircons still have positive $\varepsilon_{Hf}(t)$ values, but lower than those from the earlier stage samples. They show gradually decrease of the $\varepsilon_{Hf}(t)$ values, and display a downward trend with decreasing age of the event signature curve in addition to have short crustal incubation time (Fig. 7D-F). Subsequently, increasing zircon $\varepsilon_{Hf}(t)$ values and crustal residence ages with decreasing age appear during Early Carboniferous (ca. 359–323 Ma), with a slow decline in crustal incubation time (Fig. 7D-F). Over again, zircon $\varepsilon_{Hf}(t)$ values start to decrease signifcantly beginning in the Late Carboniferous (ca. 320 Ma). Correspondingly, the samples show a downward trend of the event signature curve through time in addition to have long crustal incubation time (Fig. 7D-F). In the Dananhu belt, finally, zircon $\varepsilon_{Hf}(t)$ values and crustal residence ages of the rocks reach their minimum values, while crustal incubation time reaches maximum values (Fig. 7D-F).

### 6.4. The Kangguer

At Late Devonian to Late Carboniferous (ca. 380 Ma to ca. 310 Ma), the rocks from the Kangguer belt were characterized by constant highly positive $\varepsilon_{Hf}(t)$ values, but low crustal incubation time, with horizontal event signature curve (Fig. 9D-F). In contrast, the zircon Hf isotope value of the rocks suddenly dropped sharply with decreasing emplacement age after ca. 310 Ma, consistent with shifts to sharp downward trend of the event signature curve but the steep increase of crustal incubation time (Fig. 9D-F).

### 6.5. The Yamansu belt

The earliest magmatic zircons of the intermediate-felsic rocks in the Yamansu belt exhibit near-zero $\varepsilon_{Hf}(t)$ values and have the longest crustal incubation time among the Paleozoic rocks in the Eastern Tianshan (Fig. 11D-F). Afterwards, the samples in the Yamansu belt possess highly positive zircon $\varepsilon_{Hf}(t)$ values and display sharp rising trends of the $\varepsilon_{Hf}(t)$ values and event signature curve through time during ca. 350 Ma to 320 Ma, whereas most of the zircons have a short crustal incubation time during this period (Fig. 11D-F). Later (ca. 310–280 Ma), the rocks can be found in the Yamansu belt with positive zircon $\varepsilon_{Hf}(t)$ values, but significantly lower than those from the earlier ones. Furthermore, the event signature curve tends to be significantly decrease with decreasing age, consistent with the fact that they have relatively long crustal incubation time at ca. 310 Ma to 280 Ma.

## 7. Temporal and spatial constraints on the evolution and final assembly of the Eastern Tianshan

The spatial-temporal variations in the composition of Paleozoic mafic–intermediate–felsic igneous rocks are prominent in the Eastern Tianshan. These variations may be caused either by differentiation effects during the partial melting of source rocks and the fractional crystallization of primitive magmas, or by the differences in the composition of source rocks. Whatever, the source rocks were generated by the Paleozoic subduction of the Kangguer oceanic slab beneath the different tectonic units for accretionary orogeny. These source rocks, in particular, intermediate-felsic rocks would occur as the orogenic lithospheric crust along the fossil convergent plate boundary in the Eastern Tianshan, with various crustal architecture involving in the crustal thickness and crustal evolution trend. In this context, there are at least four stages for the formation of Paleozoic igneous rocks with distinguishable lithology distribution, crustal thickness, and crustal evolution trend over time in different tectonic zones in the Eastern Tianshan (Figs. 2–11).

### 7.1. Initial stage of development of the Harlik–Dananhu arc system

According to recent investigations, the earliest (Middle to Late Ordovician) magmatic rocks with arc-like geochemical features have been both identified in the Harlik belt and the Dananhu belt, implying that they were both generated in an arc-related tectonic setting since Ordovician (Figs. 3 and 7; Tables S1 and S3; e.g., Deng et al., 2016; Du et al., 2018a; Zhang et al., 2018; Sun et al., 2019; Gong et al., 2023). The Harlik–Dananhu arc system has been traditionally regarded as southward subduction of the Junggar Ocean, which was reinforced by subsequent researches on tectonism and sedimentation (Charvet et al., 2007; Zhang et al., 2016). Nonetheless, there has been increasing investigations revealing that the Kangguer oceanic plate initial northward subduction occurred during the Middle Ordovician, which eventually induced the united Harlik–Dananhu arc system (Xiao et al., 2004; Zhang et al., 2018; Du et al., 2021).

The latter model is more reasonable as it can fit most of the regional geological features (Ma, 1999; Xiao et al., 2004; Zhang et al., 2017, 2018, 2020; Du et al., 2021; Mao et al., 2022a). Firstly, the oldest (Middle to Late Ordovician) arc-related magmatic rocks have been both identified in the Harlik belt and the Dananhu belt, and the arc magmatism shows a younging trend accompanied by decreasing magmatic volumes from north to south, which can be comparable to the volcanic front to the back-arc side in the Japan arc system (Kogiso et al., 2009; Du et al., 2018a, 2021; Mao et al., 2022a). Secondly, it is found that the consistence of the earliest Ordovician to Silurian sedimentary strata occurred both in the Harlik and Dananhu arcs (Ma, 1999; Zhao et al., 2022). Thirdly, lithologically, the Ordovician to Silurian strata in the

Harlik area are dominated by passive margin-like clastic sediments (Zhang et al., 2018, 2020), while those in the Dananhu area are composed mainly of active margin-like arc magmatic rocks (Xiao et al., 2004; Mao et al., 2022a). Fourthly, Early Paleozoic subduction-related porphyry copper deposits, such as the Yudai, Yuhai, and Sanchakou deposits, were found in the Dananhu arc (Sun et al., 2018; Zhang et al., 2022), while coeval porphyry deposits are lacking in the Harlik arc. Moreover, crustal thickness calculated by median Sr/Y ratio of intermediate rocks here suggests that the initial stage of the Harlik arc crust was thinner than the Dananhu crust at the same period (Figs. 3C and 7C). Finally, the Middle Ordovician intermediate-felsic rocks in the Harlik and Dananhu belt were both characterized by highly positive zircon $\varepsilon_{Hf}(t)$ values, but low crustal incubation time (Figs. 3D-F and 7D-F), arguing that they were probably derived from newly formed island arc crust with a direct addition of depleted mantle material.

The Sr/Y data compiled in this study suggest that crustal thickness of the Dananhu arc began to increase in the Middle Ordovician to Late Devonian (ca. 470–381 Ma), consistent with estimates for the progressive maturation of the Dananhu arc crust that was produced by the continuous northward subduction of the Kangguer oceanic plate (Fig. 7C). Additionally, the crustal incubation time tends to be short (<300 Ma) in the rocks during this period (Fig. 7F), implying that all the rocks are associated with juvenile materials. Therefore, the unified Dananhu–Harlik arc possibly underwent trench advance during the initial subduction of the Kangguer oceanic plate and formation of the Yudai porphyry copper deposit (450 ± 4 Ma; Sun et al., 2018) and Honghai Cu-Pb deposit (436 ± 2 Ma; Mao et al., 2019) in the Kalatage area of the Dananhu arc and the alkaline to tholeiitic basalts (440–434 Ma; Zhao et al., 2022) in the Harlik arc (Figs. 1C, 2, and 12A).

However, the zircons of the Dananhu arc rocks exhibit trends of

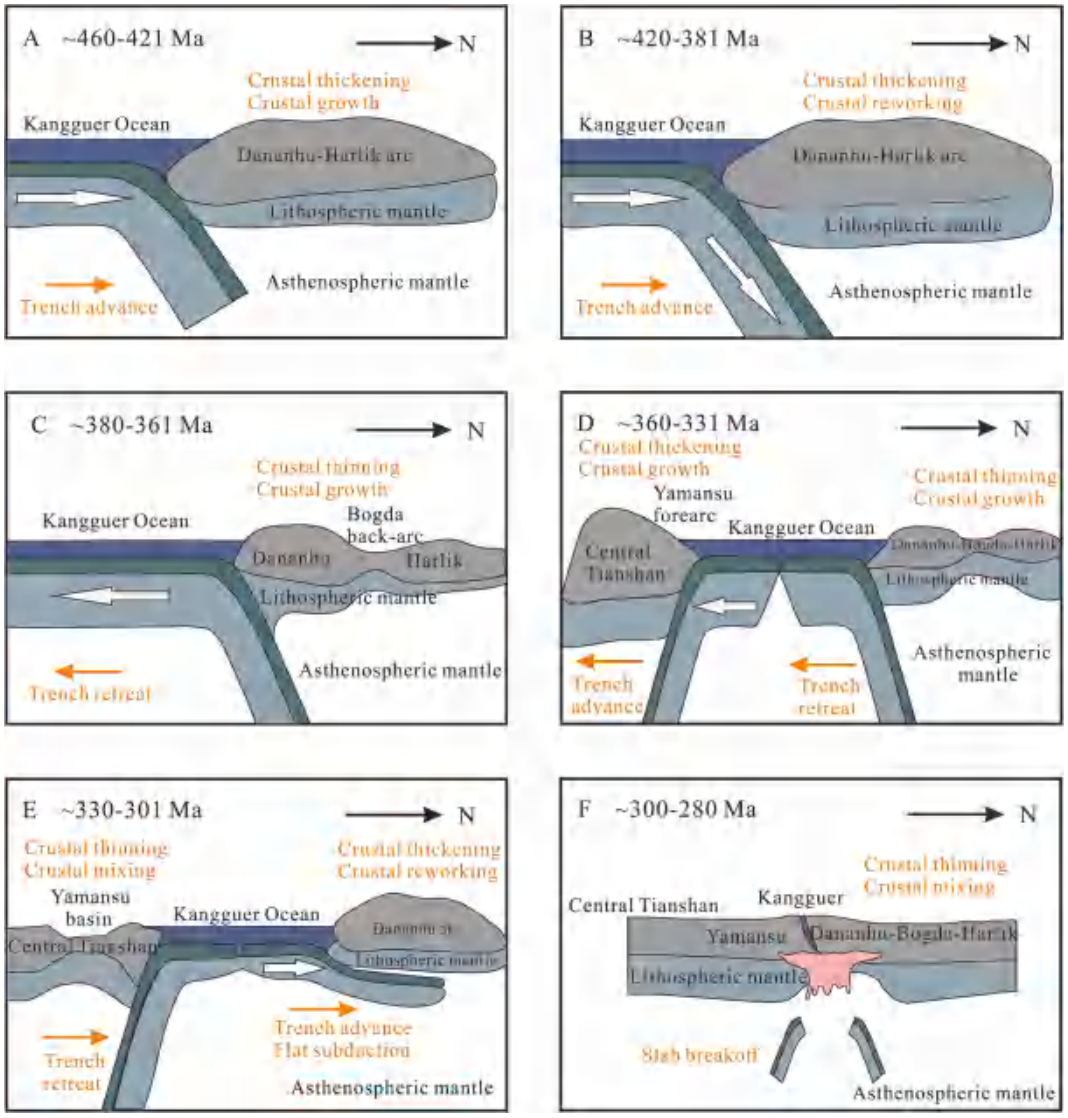


**Fig. 12.** Schematic cartoons illustrating the Paleozoic tectonic evolution of the Chinese Eastern Tianshan. (A) At ca. 460–421 Ma, initial northward subduction of the Kangguer oceanic slab led to the formation of the united Harlik–Dananhu arc system. The trench advance gave rise to the earliest crustal thickening and crustal growth event in the Harlik–Dananhu arc system. (B) During ca. 420–381 Ma, the continuous northward subduction of the Kangguer oceanic slab resulted in progressive maturation of the Dananhu arc crust. (C) At ca. 380–361 Ma, Kangguer oceanic plate southward retreat induces initial back-arc rifting occurred on the Dananhu side. (D) During ca. 360–331 Ma, the Kangguer oceanic slab persistently southward rollback gave rise to regional extension and establishment of the Bogda back-arc basin, and southward subduction of the Kangguer Ocean beneath the Central Tianshan Block built the Yamansu arc. (E) At ca. 330–301 Ma, the renewed northward subduction of the Kangguer oceanic plate beneath the Dananhu arc forced the southward subducting slab beneath the Yamansu arc to trigger a northward rollback, which resulted in the extension of the overlying Yamansu arc crust and caused the tectonic transformation into back-arc basin. (F) During ca. 300–280 Ma, the Eastern Tianshan entered into a post-collisional setting following the closure of the Kangguer Ocean.

increasing $\varepsilon_{Hf}(t)$ with decreasing age before ca. 420 Ma and then decreasing $\varepsilon_{Hf}(t)$ subsequently, consistent with displaying rising trends of the event signature curve before ca. 420 Ma and then to downward trends thereafter (Fig. 7D-E). This led to the transition of the source from an input of juvenile mantle material directly forming the Dananhu intraoceanic arc crust before ca. 420 Ma to generated by reworking of the juvenile arc crust after ca. 420 Ma, and is consistent with arc magmatism in the Harlik arc ceased after ca. 420 Ma (Figs. 3 and 7). The increasing crustal thickness and decreasing $\varepsilon_{Hf}(t)$ values through time until ca. 381 Ma (Fig. 7C-D) refer to the crustal reworking via subduction trench advancing, triggering the compressional thickening in the overriding plate and the formation of some other porphyry copper deposits (e.g., Sanchakou: 416 Ma; Zhang et al., 2022) and possibly skarn-type deposits (e.g., Xierqu: 382 ± 2 Ma; Mao et al., 2018) in the Dananhu arc (Fig. 12B).

### 7.2. Southward movement of the Kangguer Ocean responsible for the Bogda back-arc basin and the Yamansu continental marginal arc

Following the progressive thickening of the Dananhu arc crust through the history of accretion in the Middle Ordovician to Late Devonian (ca. 470–381 Ma), the crustal thickness shifts to thinning after ca. 380 Ma in which calculated by median Sr/Y ratio of intermediate rocks from the Dananhu belt (Fig. 7C). The first episode of crustal thinning (ca. 380–350 Ma) of the Dananhu arc was associated with the adjacent crustal thinning through time (ca. 345–330 Ma) at the center part of the Dananhu–Harlik arc, and probably relate to the opening of the Bogda back-arc basin (Chen et al., 2013; Zhang et al., 2017).

Field relations and geochemical evidence of magmatism provide further support for extensional regime prevailed during this period in the north Eastern Tianshan (Fig. 12C). For examples, (a) voluminous ca. 380–357 Ma high-Al mafic and A-type felsic magmatism in the Dananhu segment (Mao et al., 2022a; Du et al., 2023), as well as ca. 352–351 Ma A-type granites in the Harlik belt (Liu et al., 2022), which are emplaced in an extensional setting coupled with mantle upwelling, and (b) development of Bogda intra-arc basins characterized by ca. 345–330 Ma bimodal volcanic rocks that formed by rising asthenosphere caused the rifting of the overriding plate in an extensional setting (Chen et al., 2013; Zhang et al., 2017). More widely, Collins et al. (2011) noted that in what they termed external orogenic systems, such as those around the Pacific rim, the range in Hf isotope ratios narrowed and trended towards more radiogenic values through time. This is similar to the trends recognized here, i.e., the samples exhibit trends of increasing $\varepsilon_{Hf}(t)$ with decreasing age at ca. 350–330 Ma for the Harlik segment, at ca. 345–330 Ma for the Bogda back-arc basin, and ca. 360–330 Ma for the Dananhu belt (Figs. 3, 5, and 7), corresponding to the magmatic migration from the Dananhu arc to the Bogda and Harlik side (Chen et al., 2013; Zhang et al., 2017; Liu et al., 2022; Mao et al., 2022a; Du et al., 2023). An analogous driving mechanism of back-arc basin formation has been recognized in the concentration of back-arc basins in the western Pacific margins (Sdrolias and Müller, 2006; Magni, 2019; Grevemeyer et al., 2021).

The leading hypothesis for intraoceanic arc crustal thinning is thought to be due to episodes of lower crustal delamination occurring after significant crustal thickening, and a sequence or tectonic switching model is thought to occur cyclically in long-lived arcs, such as the Coast mountains, Sierra Nevada, etc. (Collins, 2002; Chapman et al., 2015; Profeta et al., 2015). This model proposed a long-term slab retreat that causes arc splitting and the opening of intra−/back-arc basins, which likely signifies mantle upwelling to relatively shallow levels during lithospheric extension (Collins, 2002; Chapman et al., 2015; Profeta et al., 2015; Tang et al., 2017). Hence, the most suitable model could be the southward rollback of the downgoing Kangguer oceanic plate, which caused the extension of the overriding Dananhu–Harlik arc crust and possibly development of the Bogda back-arc basin. The retreating subduction have promoted the overprinting mineralization in the Sanchakou–Yuhai copper deposits (360–350 Ma; Zhang et al., 2022) and the Xiaorequanzi VMS mineralization (357–354 Ma; Mao et al., 2020) in the Dananhu arc.

Meanwhile, the subduction trench also southward moved towards the Central Tianshan Block, as evidenced by the identifcation of the earliest arc magmatism in the Kangguer and Yamansu belts (Fig. 12D; Tables S4 and S5). The Kangguer belt remained relatively constant during the Late Devonian to Early Carboniferous (ca. 360–330 Ma), and the igneous magmatism is characterized by granites (Wang et al., 2014; Du et al., 2019b). The rocks in the Kangguer belt have homogeneous high $\varepsilon_{Hf}(t)$ values and horizontal event signature curve through this period, with moderate crustal incubation time, implying they probably originate from a mixing juvenile source, in accordance with the interpretation for the accretionary prism.

As a contrast, the igneous magmatism from ca. 350 Ma to 330 Ma in the Yamansu belt is characterized by a variety of rock types, such as high-K calc-alkaline granites and diorites, as well as continental arc basalts and andesites (Table S5). The earliest magmatic zircons of the intermediate-felsic rocks in the Yamansu belt exhibit lowest $\varepsilon_{Hf}(t)$ values and have the longest crustal incubation time among the Paleozoic rocks in the Eastern Tianshan. This implies a heterogeneous source or magma mixing of ancient supracrustal and juvenile/mantle-derived materials (Belousova et al., 2006, 2010). The relatively stable crustal architecture and enhanced continental input revealed by low zircon $\varepsilon_{Hf}(t)$ values of the Yamansu rocks argue against any petrogenetic intimacy of the rocks in this belt to those in the north Eastern Tianshan. Therefore, the previous proposal that the Yamansu arc was formed from the arc migration due to the slab retreat of a long-lived northward subduction (Xiao et al., 2004, 2008) can be ruled out.

Moreover, inherited zircons from the igneous rocks and detrital zircons from sandstones in the Yamansu belt have distinct Proterozoic cluster around 1400–1600 Ma (Luo et al., 2012; Chen et al., 2019, 2020; Long et al., 2020), which is absent in other nearby Precambrian blocks but the Central Tianshan block (Long and Huang, 2017; Chen et al., 2019, 2020), indicating the basement of the Yamansu belt is composed of Precambrian basement rocks of the Central Tianshan block (Luo et al., 2012; Du et al., 2018b, 2018c; Chen et al., 2019, 2020; Long et al., 2020). In this scene, an Early Carboniferous Yamansu continental marginal arc was built along the Central Tianshan Block related to the southward subduction of the Kangguer oceanic slab is prefered here. This posibility is in good agreement with the abrupt increase in crustal thickness with decreasing age at ca. 350 Ma to 330 Ma, as well as the increase in zircon $\varepsilon_{Hf}(t)$ values, sharp rising trends of the event signature curve, and the decrease in crustal incubation time during this period (Fig. 11).

### 7.3. The second episode of northward migration of the Kangguer oceanic plate

Taken together all the Paleozoic igneous rocks occurred in the Eastern Tianshan, the earlier rocks with emplacement age before ca. 330 Ma mainly exposed in the Dananhu belt and the Harlik belt, even though some ca. 360–330 Ma rocks can be observed in the Bogda belt, the north of the Kangguer belt, and the Yamansu belt, but the magmatic rocks formed after ca. 330 Ma are widely developed throughout the Eastern Tianshan (Figs. 2–11; Tables S1-S5; e.g., Deng et al., 2016; Zhang et al., 2018; Sun et al., 2019; Du et al., 2021, 2023; Mao et al., 2022a, 2022b; Gong et al., 2023). In each area the crustal thickness exhibit broadly similar patterns during the Late Carboniferous (ca. 330–300 Ma). For instance, the timing of maximum crustal thickening in the Bogda belt, Kangguer belt, and Yamansu belt is constrained at ca. 330–300 Ma, though we cannot be certain that the crustal thickness of the Yamansu belt at 305 Ma reaches its peak thickness due to there are no data available after 305 Ma (Figs. 5, 9, and 11). These estimates are in broad agreement with the Sr/Y data that suggest the submaximum crustal thicknesses at ca. 330 Ma and 320 Ma for the Harlik belt and

Dananhu belt, respectively (Figs. 3 and 7).

Besides, the zircons from the Harlik–Bogda–Dananhu intermediate-felsic rocks show large variations in $\varepsilon_{Hf}(t)$ values and have wide range of crustal residence ages as well as crustal incubation time at ca. 330–300 Ma (Figs. 3, 5, and 7). Considering that these zircons have slightly primitive $\varepsilon_{Hf}(t)$ values, generation both by addition of juvenile material and reworking of the pre-existing arc crust has been suggested to be a possible mechanism for these rocks (Gong et al., 2023; Wang et al., 2023). Hence, the renewed northward subduction of the Kangguer oceanic slab to be the most likely geodynamic background. This is further documented by the widely developed of Late Carboniferous rocks throughout the Harlik–Bogda–Dananhu arc system and display typical arc magmatic trace element patterns (Xiao et al., 2017; Wang et al., 2018; Du et al., 2019a). Moreover, the northward advance of the Kangguer oceanic plate towards the Harlik–Bogda–Dananhu system probabaly forced by flat subduction, based on relatively enriched in adakitic rocks in the Dananhu belt during this period (Fig. 12E; Xiao et al., 2017; Wang et al., 2018; Du et al., 2019a). Concurrent with the flat subduction is the formation and overprinting mineralization of the Tuwu-Yandong copper deposits (336–324 Ma; Wang et al., 2018; Song et al., 2018; Gong et al., 2023).

On the other hand, the possible maximum crustal thickening of Yamansu belt is culminated with median 32.3 km thick crust at ca. 310 Ma, but this crust thickness is much lower than those of the Dananhu belt at the same time (49.1 km) (Figs. 7 and 11; Tables S3 and S5). Besides, the rocks formed at this stage in the Yamansu belt possess highly positive zircon $\varepsilon_{Hf}(t)$ values and most of the zircons have a short crustal incubation time, implying another direct addition of depleted mantle material event occurred in the Eastern Tianshan. This event is also documented by the whole-rock Nd isotopic data of the Late Carboniferous granitic plutons in this belt that have highly positive $\varepsilon_{Nd}(t)$ values and juvenile model ages (Zhang et al., 2016; Zhao et al., 2019a, 2019b). Thus, it can be speculated that the renewed northward subduction of the Kangguer oceanic plate beneath the Dananhu arc probably drag the southward subducting slab beneath the Yamansu arc to have a northward rollback, which would cause the extension of the overlying Yamansu arc crust and result in the tectonic transformation into back-arc basin. Correspondingly, this extensional event coincides with the formation of several Fe-Cu deposits (e.g., Duotoushan, Heijianshan, and Yamansu; Hou et al., 2014; Zhao et al., 2019a) in the Yamansu belt.

### 7.4. Post-collisional extension of the Eastern Tianshan

The Kangguer Ocean was closed in the latest Carboniferous and the subduction setting shifted to post-collisional extension probably occurred at the earliest Permian, which is favored to account for the regional sedimentation, tectonism, and magmatism based on several previously geological studies (Fig. 12F; Han and Zhao, 2018; Zhang et al., 2018; Du et al., 2021; Wang et al., 2022; Gong et al., 2023). Firstly, the presence of detrital zircons from the Early Permian and Triassic sandstones in the Dananhu arc reveals a provenance from the Yamansu–Central Tianshan block and thus provides robust evidence for the closure of the Kangguer Ocean and subsequent collision between the Central Tianshan block and the North Tianshan Belt at some time before Early Permian (Zhang et al., 2016; Chen et al., 2020). Secondly, ca. 300 Ma shear zone-hosted Au deposits, as well as structural and chronological analyses in the Kangguer suture, reveal that a transition from subduction-accretion to post-collisional transcurrent setting probably took place in the earliest Permian (Xiao et al., 2004; Wang et al., 2014). Thirdly, the Early Permian red molasse sequence, coupled with coeval overthrust or strike-slip shearing in the Bogda area, indicates the termination of a marine setting and the beginning of a welded terrestrial environment in the Eastern Tianshan (Shu et al., 2005). Finally, post-collisional extensional magmatism widely occur in the Eastern Tianshan at this epoch (ca. 300–280 Ma), such as Balikun Nb-enriched gabbros and A-type granites in the Harlik belt (Yuan et al., 2010), Qijiaojing bimodal volcanic rocks and Hongshankou Nb-enriched dolerites in the Bogda belt (Zhang et al., 2020), Sha'erhu A-type granites in the Dananhu belt (Mao et al., 2014), mafic–ultramafic rocks in the Kangguer belt (Xiao et al., 2004; Qin et al., 2011), and Dikan'er Nb-rich basalts and Aqishan mountain A-type granites in the Yamansu belt (Du et al., 2018b; Zhang et al., 2020), etc.

This posibility is in accordance with the available data in this study. For instance, the second episode of crustal thinning in the Eastern Tianshan at ca. 300–280 Ma involved the Bogda belt, Dananhu belt, and the Kangguer belt in addition to all the samples from the Eastern Tianshan displays significantly decrease in zircon $\varepsilon_{Hf}(t)$ values and event signature curve and has long crustal incubation time during this stage (Figs. 5, 7, and 9), reflecting some sort of lithospheric extension and a heterogeneous source or magma mixing of ancient supracrustal and juvenile/mantle-derived materials (Belousova et al., 2006, 2010).

### 7.5. Implications for crustal architecture and its evolution

Spatial-temporal variations in lithology composition, crustal thickness, and crustal evolution trend have shown that the Eastern Tianshan trench-arc-basin system underwent repeated tectonic switches (Fig. 12). It is worth noting that such tectonic switches are exceptionally to occur cyclically in long-lived arcs, based on numerical modeling studies and regional examples (e.g., Profeta et al., 2015; Spencer et al., 2019), but further geological evidence is needed to test and verify this model for the slab dynamics of the Eastern Tianshan trench-arc-basin system. Meanwhile, extensive crustal growth probably took place during the repeated tectonic switches (Sengör et al., 1993; Jahn et al., 2004; Cawood et al., 2009; Kröner et al., 2014; Tang et al., 2017; Wang et al., 2022). Unlike the temporal tectonic-magmatic evolution of the continental arcs, with crustal growth dominating at extensional stages (Ducea and Barton, 2007; Kemp et al., 2009; Chapman and Ducea, 2019), two processes are believed to envisage the generation of continental crust in the accretionary orogens, i.e., vertical growth, which comprises over- and underplating of magmatic melts, and lateral growth, which basically involves the accretion of arc complexes or oceanic plateaus (Sengör et al., 1993; Jahn et al., 2004; Cawood et al., 2009; Kröner et al., 2014; Tang et al., 2017; Wang et al., 2022).

Since the growth of crust envisages the directly addition of mantle-derived material to the crust, the magmatic rocks formed during the crustal growth stages are characterized by high and increasing zircon $\varepsilon_{Hf}(t)$ values, rising trend of event signature curve, in addition to most of the magmatic zircons have a short crustal incubation time (Figs. 2–11). Both crustal growth patterns indeed can be documented in the Eastern Tianshan, but the compiled data here show that the proportion occupied by crustal growth is limited. Such trends can only be found in the arc magmatic rocks formed at initial compressional advancing stages in the Dananhu belt (ca. 460–421 Ma) and the Yamansu belt (ca. 360–331 Ma), accompanied by significant crustal thickening, and during back-arc extensional stage (ca. 380–331 Ma) in the Dananhu–Bogda–Harlik arc system with crustal thinning (Figs. 2–11). Whereas the rest of the magmatic rocks in the Eastern Tianshan are characterized by decreasing zircon $\varepsilon_{Hf}(t)$ values or display a downward trend with decreasing age of the event signature curve, which generally suggests processes such as crustal reworking or mixing between two source components.

The above trends demonstrate that subduction zone initial advance enhanced the generation of new crust, probably via mantle-derived magma lateral accretion, in accordance with significant crustal thickening of the Dananhu belt during ca. 460–421 Ma and for the Yamansu belt at ca. 360–331 Ma (Figs. 2–12). Inversely, as progressive maturation of the arc crust evidenced by the sharp increase of crustal thickness in the Dananhu belt at ca. 420–381 Ma and the Yamansu belt at ca. 330–330 Ma, magmatic rocks generated during episodes of continuous subduction of the Kangguer Ocean show gradually decrease of the $\varepsilon_{Hf}(t)$ values, and display a downward trend with decreasing age of the event

signature curve in addition to have longer crustal incubation time, suggesting they probably generated by reworking of the juvenile arc crust. Changes in the magma sources with continuous subduction of the Kangguer Ocean at ca. 370–300 Ma can be observed in the Kangguer belt as the rocks show an intermediate slope of the $\varepsilon_{Hf}(t)$ values and event signature curve. This widely variable isotopic characteristic represents a typical mixing of mantle-derived melts and crustal materials. While the formation of continental crust by the latter two mechanisms cannot account for crustal growth (Wang et al., 2023).

Another significant crustal growth event occurred at back-arc extensional stage (ca. 380–331 Ma) in the Dananhu–Bogda–Harlik arc system. The back-arc related-rocks possess highly positive zircon $\varepsilon_{Hf}(t)$ values and display sharp rising trends of event signature curve in the Dananhu–Bogda–Harlik arc system indicates vertical growth by underplating/overplating of mantle-derived magma. By comparison, in each area the post-collisional extensional magmatism exhibits broadly similar patterns and shows significantly decrease of the zircon $\varepsilon_{Hf}(t)$ values and the event signature curve, but exhibits trends of increasing crustal incubation time with decreasing age, suggesting that they were probably formed from mixtures of mantle-derived melts and ancient crustal materials from the Central Tianshan basement. The above evidence further suggest the accretion/collision of the different belts of the Eastern Tianshan was basically contemporaneous, with all experiencing a post-collisional episode during ca. 300–280 Ma, and the post-collisional episode was predominantly characterized by crustal reworking of both juvenile and ancient crustal components.

## 8. Concluding remarks

The systematic data compilation and analyses reveal that the Paleozoic magmatism in the Chinese Eastern Tianshan display marked temporal-spatial variations in geochemical and isotopic compositions. Variations in crucial geochemical-isotopic signatures have proven to be effective in developing crustal and tectonic activities of multiple accreting units and quantifying the crustal formation model in an evolving accretionary orogen. According to these spatial-temporal variations in compositions and crustal thickness as well as the other geological observations, we conclude that:

(1) Most mafic–intermediate–felsic magmatism in the Chinese Eastern Tianshan are concentrated into relatively short time periods between ca. 360–280 Ma, and the Dananhu–Harlik arc system tend to be characterized by one more dominant period of magma emplacement at ca. 460–420 Ma.

(2) The variations in crustal thickness are different in the five segments of the Eastern Tianshan. For instance, the Dananhu belt had experienced two phases of crustal thickening during ca. 460–381 Ma and 360–321 Ma, separated by periods of crustal thinning at ca. 380–361 Ma and 320–280 Ma, however, the timing of maximum crustal thickening in the Harlik, Bogda, Kangguer, and Yamansu are constrained to ca. 450 Ma, 320 Ma, 330 Ma, and 310 Ma, respectively.

(3) Repeated tectonic switches of the Eastern Tianshan trench-arc-basin system during subduction of the Kangguer oceanic plate are recorded by the spatial-temporal variations of magmatism and crustal thickness. Generally, the periods of trench advance tend to be associated with higher magmatic activities coupled with crustal thickening, in contrast to the trench retreat that is characterized by crustal thinning with different magma volumes in the different belts. Thus, the northern trench of the Kangguer Ocean had experienced two phases of trench northward advance (ca. 470–381 Ma and 330–301 Ma, respectively) and an intervening trench retreat (ca. 380–331 Ma). Meanwhile, the southern trench of the Kangguer Ocean had experienced trench southward advance and northward retreat at ca. 370–331 Ma and 330–301 Ma, respectively. Then, the Kangguer Ocean was closed in the latest Carboniferous and the subduction setting shifted to post-collisional extension probably occurred at the earliest Permian.

(4) Trench advance accompanied by significant crustal thickening has induced crustal growth in Eastern Tianshan, such as northern trench advance at ca. 460–421 Ma and southern trench advance at ca. 360–331 Ma, respectively. The northern trench retreat with crustal thinning during ca. 380–331 Ma has induced crustal growth in the Dananhu–Bogda–Harlik arc system. The rest of the magmatic rocks in the Eastern Tianshan are characterized by crustal reworking or mixing.

## Declaration of competing interest

The authors declare that they have no known competing financial interests or personal relationships which have or could be perceived to have influenced the work reported in this article.

## Data availability

The data that has been used is confidential.

## Acknowledgements

Constructive comments from anonymous reviewers are greatly appreciated. Professor Yildirim Dilek (Editor-in-Chief) and Professor Wenjiao Xiao (Guest Editor) are thanked for editorial input and efficient handling. Financial support was provided by the National Key Research and Development Project (2019YFA0708601), the National Natural Science Foundation of China (42373048 and U1906207), and the Opening Foundation of State Key Laboratory of Continental Dynamics, Northwest University (22LCD07).

## Appendix A. Supplementary data

Supplementary data to this article can be found online at https://doi.org/10.1016/j.earscirev.2024.104761.

## References

Ao, S.J., Mao, Q.G., Windley, B.F., Song, D.F., Zhang, Z.Y., Zhang, J.E., Wan, B., Han, C. M., Xiao, W.J., 2021. The youngest matrix of 234 Ma of the Kanguer accretionary mélange containing blocks of N-MORB basalts: Constraints on the northward subduction of the Paleo-Asian Kanguer Ocean in the Eastern Tianshan of the southern Altaids. Int. J. Earth Sci. 110, 791–808.

Armstrong, R.L., 1981. Radiogenic isotopes, the case for crustal recycling on a near-steady state no-continental-growth Earth. Philos. Trans. Roy. Soc. London. Ser. A Math. Phys. Sci. 301, 443–472.

Belousova, E.A., Griffn, W.L., O'Reilly, S.Y., 2006. Zircon crystal morphology, trace element signatures and Hf isotope composition as a tool for petrogenetic modelling: examples from eastern Australian granitoids. J. Petrol. 47, 329–353.

Belousova, E.A., Reid, A.J., Griffin, W.L., O'Reilly, S.Y., 2009. Rejuvenation vs. recycling of Archean crust in the Gawler Craton, South Australia: evidence from U–Pb and Hf isotopes in detrital zircon. Lithos 113, 570–582.

Belousova, E.A., Kostitsyn, Y.A., Griffn, W.L., Begg, G.C., O'Reilly, S.Y., Pearson, N.J., 2010. The growth of the continental crust: constraints from zircon Hf-isotope data. Lithos 119, 457–466.

Beltrando, M., Hermann, J., Lister, G., Compagnoni, R., 2007. On the evolution of orogens: pressure cycles and deformation mode switches. Earth Planet. Sci. Lett. 256, 372–388.

BGMRXUAR (Bureau of Geology and Mineral Resources of Xinjiang Uygur Autonomous Region), 1993. Regional Geology of Xinjiang Uygur Autonomous Region. Geological Publishing House, pp. 1–841 (in Chinese).

Boekhout, F., Roberts, N.M.W., Gerdes, A., Schaltegger, U., 2013. A Hf-isotope perspective on continent formation in the south Peruvian Andes. Geol. Soc. Lond. Spec. Publ. 389, 305–321.

Cao, F.G., Tu, Q.J., Zhang, X.M., Ren, Y., Li, S.L., Dong, F.R., 2006. Preliminary determination of the Early Paleozoic magmatic arc in the Karlik Mountains, East Tianshan, Xinjiang, China-evidence from zircon SHRIMP U-Pb dating of granite bodies in the Tashuihe area. Geol. Bull. China 25, 923–927 (in Chinese with English abstract).

Cao, M.J., Qin, K.Z., Li, G.M., Evans, N.J., McInnes, B.I.A., Lu, W.W., Deng, G., 2017. Petrogenesis of the Baishan granite stock, Eastern Tianshan, NW China: geodynamic setting and implications for potential mineralization. Lithos 292–293, 278–293.

Cawood, P.A., Kröner, A., Collins, W.J., Kusky, T.M., Mooney, W.D., Windley, B.F., 2009. Accretionary orogens through Earth history. Geol. Soc. Lond. Spec. Publ. 318, 1–36.

Cawood, P.A., Hawkesworth, C.J., Dhuime, B., 2013. The continental record and the generation of continental crust. Geol. Soc. Am. Bull. 125, 14–32.

Chapman, J.B., Ducea, M.N., 2019. The role of arc migration in Cordilleran orogenic cyclicity. Geology 47, 627–631.

Chapman, J.B., Ducea, M.N., DeCelles, P.G., Profeta, L., 2015. Tracking changes in crustal thickness during orogenic evolution with Sr/Y: an example from the North American Cordillera. Geology 43, 919–922.
Charvet, J., Shu, L.S., Laurent-Charvet, S., 2007. Paleozoic structural and geodynamic evolution of eastern Tianshan (NW China): welding of the Tarim and Junggar plates. Episodes 30, 162–186.
Charvet, J., Shu, L.S., Laurent-Charvet, S., Wang, B., Faure, M., Cluzel, D., Chen, Y., Jong, K.D., 2011. Palaeozoic tectonic evolution of the Tianshan belt, NW China. Sci. China-Earth Sci. 54, 166–184.
Chen, X.J., Shu, L.S., Santosh, M., 2011. Late Paleozoic post-collisional magmatism in the Eastern Tianshan Belt, Northwest China: new insights from geochemistry, geochronology and petrology of bimodal volcanic rocks. Lithos 127, 581–598.
Chen, X.J., Shu, L.S., Santosh, M., Zhao, X.X., 2013. Island arc-type bimodal magmatism in the Eastern Tianshan Belt, Northwest China: geochemistry, zircon U-Pb geochronology and implications for the Paleozoic crustal evolution in Central Asia. Lithos 168–169, 48–66.
Chen, X.J., Zhang, K.H., Zhou, J., 2016. Geochronology and geochemistry characteristics of the Early Permian monzogranite and dioritic enclaves of East Tianshan and their tectonic implications. Acta Geol. Sin. 90, 2334–2354 (in Chinese with English abstract).
Chen, Z.Y., Xiao, W.J., Windley, B.F., Schulmann, K., Mao, Q.G., Zhang, Z.Y., Zhang, J.E., Deng, C., Song, S.H., 2019. Composition, Provenance, and Tectonic Setting of the Southern Kangurtag Accretionary Complex in the Eastern Tianshan, NW China: implications for the Late Paleozoic Evolution of the North Tianshan Ocean. Tectonics 38, 2779–2802.
Chen, Y., Wang, G.C., Shen, T.Y., Zhang, P., Sotiriou, P., Zhu, C.Y., 2020. Tectono-geomorphic evolution of Harlik Mountain in the Eastern Tian Shan, insight from thermochronological data and geomorphic analysis. Geol. J. 55, 7322–7334.
Chung, S.L., Chu, M.F., Zhang, Y., Xie, Y., Lo, C.H., Lee, T.Y., Lan, C.Y., Li, X.H., Zhang, Q., Wang, Y., 2005. Tibetan tectonic evolution inferred from spatial and temporal variations in post-collisional magmatism. Earth Sci. Rev. 68, 173–196.
Collins, W.J., 2002. Hot orogens, tectonic switching, and creation of continental crust. Geology 30, 535–538.
Collins, W.J., Belousova, E.A., Kemp, A.I.S., Murphy, J.B., 2011. Two contrasting Phanerozoic orogenic systems revealed by hafnium isotope data. Nat. Geosci. 4, 333–337.
Condie, K.C., 1998. Episodic continental growth and supercontinents. A mantle avalanche connection? Earth Planet. Sci. Lett. 163, 97–108.
Condie, K.C., 2007. Accretionary orogens in space and time. In: Hatcher Jr., R.D., Carlson, M.O., McBride, J.H., Martínez Catalán, J.R. (Eds.), 4-D Framework of Continental Crust: Geological Society of America Memoir 200.
DeCelles, P.G., Ducea, M.N., Kapp, P., Zandt, G., 2009. Cyclicity in Cordilleran orogenic systems. Nat. Geosci. 2, 251–257.
Defant, M.J., Drummond, M.S., 1990. Derivation of some modern arc magmas by melting of young subducted lithosphere. Nature 347, 662–665.
Deng, Y.F., Song, X.Y., Hollings, P., Zhou, T.F., Yuan, F., Chen, L.M., Zhang, D.Y., 2015. Role of asthenosphere and lithosphere in the genesis of the Early Permian Huangshan mafic-ultramafic intrusion in the Northern Tianshan, NW China. Lithos 227, 241–254.
Deng, X.H., Wang, J.B., Pirajno, F., Wang, Y.W., Li, Y.C., Li, C., 2016. Re–Os dating of chalcopyrite from selected mineral deposits in the Kalatag district in the eastern Tianshan Orogen, China. Ore Geol. Rev. 77, 72–81.
Dhuime, B., Hawkesworth, C.J., Cawood, P.A., Storey, C.D., 2012. A change in the geodynamics of continental growth 3 billion years ago. Science 335, 1334–1340.
Dong, Y.P., Zhang, G.W., Neubauer, F., Liu, X.M., Hauzenberger, C., Zhou, D.W., Li, W., 2011. Syn- and post-collisional granitoids in the Central Tianshan orogen: geochemistry, geochronology and implications for tectonic evoution. Gondwana Res. 20, 568–581.
Du, L., Long, X.P., Yuan, C., Zhang, Y.Y., Huang, Z.Y., Sun, M., Zhao, G.C., Xiao, W.J., 2018a. Early Paleozoic dioritic and granitic plutons in the Eastern Tianshan Orogenic Belt, NW China: constraints on the initiation of a magmatic arc in the Southern Central Asian Orogenic Belt. J. Asian Earth Sci. 153, 139–153.
Du, L., Long, X.P., Yuan, C., Zhang, Y.Y., Huang, Z.Y., Wang, X.Y., Yang, Y.H., 2018b. Mantle contribution and tectonic transition in the Aqishan-Yamansu Belt, Eastern Tianshan, NW China: insights from geochronology and geochemistry of Early Carboniferous to Early Permian felsic intrusions. Lithos 304–307, 230–244.
Du, L., Long, X.P., Yuan, C., Zhang, Y.Y., Huang, Z.Y., Sun, M., Xiao, W.J., 2018c. Petrogenesis of Late Paleozoic diorites and A-type granites in the central Eastern Tianshan, NW China: response to post-collisional extension triggered by slab breakoff. Lithos 318–319, 47–59.
Du, L., Yuan, C., Li, X.-P., Zhang, Y.Y., Huang, Z.Y., Long, X.P., 2019a. Petrogenesis and geodynamic implications of the Carboniferous granitoids in the Dananhu Belt, Eastern Tianshan Orogenic Belt. J. Earth Sci. 30, 1243–1252.
Du, L., Zhang, Y.Y., Huang, Z.Y., Li, X.-P., Yuan, C., Wu, B., Long, X.P., 2019b. Devonian to Carboniferous tectonic evolution of the Kangguer Ocean in the Eastern Tianshan, NW China: insights from three episodes of granitoids. Lithos 350–351, 105243.
Du, L., Zhu, H.L., Yuan, C., Zhang, Y.Y., Huang, Z.Y., Li, X.-P., Long, X.P., 2021. Paleozoic crustal evolution and tectonic switching in the Northeastern Tianshan: insights from zircon Hf isotopes of granitoids. J. Geol. Soc. Lond. 178 jgs2020–035.
Du, L., Long, X.P., Yuan, C., Zhang, Y.Y., Huang, Z.Y., Zhu, H.L., 2023. Identification of the Late Devonian back-arc magmatism in the Chinese Eastern Tianshan. Lithos 454–455, 107283.
Ducea, M.N., Barton, M.D., 2007. Igniting flare-up events in Cordilleran arcs. Geology 35, 1047–1050.
Gao, J., Qian, Q., Long, L.L., Zhang, X., Li, J.L., Su, W., 2009. Accretionary orogenic process of Western Tianshan, China. Geol. Bull. China 28, 1804–1816 (in Chinese with English abstract).
Gao, J.G., Li, W.Y., Zhou, Y., Liu, J.C., Fan, T.B., Lu, L., Zhou, R.H., 2013. Geochemistry, zircon U–Pb ages and geological significance of the Liushugou Formation rhyolite in the Sepikou region, eastern Bogda, Xinjiang. Geol. Explor. 49, 665–675.
Gong, L., Chen, H.Y., Wang, Q., Xiao, B., Zhang, S.L., Tang, G.J., 2023. Multiple tectonic switches in the Eastern Tianshan, Central Asian Orogenic Belt: implications for crustal growth and metallogenesis. Lithos 454–455, 107235.
Grevemeyer, I., Kodaira, S., Fujie, G., Takahashi, N., 2021. Structure of oceanic crust in back-arc basins modulated by mantle source heterogeneity. Geology 49, 468–472.
Griffin, W.L., Belousova, E.A., Shee, S.R., Pearson, N.J., O'Reily, S.Y., 2004. Archean crustal evolution in the northern Yilgarn Craton: U–Pb and Hf-isotope evidence from detrital zircons. Precambrian Res. 13l, 23l–282l.
Griffin, W.L., Belousova, E.A., Walters, S.G., O'Reilly, S.Y., 2006. Archaean and Proterozoic crustal evolution in the Eastern Succession of the Mt Isa district, Australia: U-Pb and Hf-isotope studies of detrital zircons. Aust. J. Earth Sci. 53, 125–149.
Guo, H.C., Zhong, L., Li, L.Q., 2006. Zircon SHRIMP U–Pb dating of quartz diorite in the Koumenzi area, Karlik Mountains, East Tianshan, Xinjiang, China, and its geological significance. Geol. Bull. China 25, 928–931 (in Chinese with English abstract).
Han, Y.G., Zhao, G.C., 2018. Final amalgamation of the Tianshan and Junggar orogenic collage in the southwestern Central Asian Orogenic Belt: constraints on the closure of the Paleo-Asian Ocean. Earth Sci. Rev. 186, 129–152.
Han, C.M., Xiao, W.J., Zhao, G.C., Mao, J.W., Li, S.Z., Yan, Z., Mao, Q.G., 2006. Major types, characteristics and geodynamic mechanism of Late Paleozoic copper deposits in Northern Xinjiang, Northwestern China. Ore Geol. Rev. 28, 308–328.
Han, C.M., Xiao, W.J., Zhao, G.C., Ao, S.J., Zhang, J., Qu, W.J., Du, A.D., 2010. In-situ U-Pb, Hf and Re-Os isotopic analyses of the Xiangshan Ni-Cu-Co deposit in Eastern Tianshan (Xinjiang), Central Asia Orogenic Belt: constraints on the timing and genesis of the mineralization. Lithos 120, 547–562.
He, Z.Y., Klemd, R., Zhang, Z.M., Zong, K.Q., Sun, L.X., Tian, Z.L., Huang, B.T., 2015. Mesoproterozoic continental arc magmatism and crustal growth in the eastern Central Tianshan Arc Terrane of the southern Central Asian Orogenic Belt: geochronological and geochemical evidence. Lithos 236, 74–89.
Hou, T., Zhang, Z.C., Santosh, M., Encarnacion, J., Zhu, J., Luo, W.Q., 2014. Geochronology and geochemistry of submarine volcanic rocks in the Yamansu iron deposit, Eastern Tianshan Mountains, NW China: constraints on the metallogenesis. Ore Geol. Rev. 56, 487–502.
Hu, A.Q., Zhang, G.X., Zhang, Q.F., Chen, Y.B., 1998. Constraints on the age of basement and crustal growth in Tianshan Orogen by Nd isotopic composition. Sci. China Ser. D Earth Sci. 41, 648–657.
Hu, F., Ducea, M.N., Liu, S., Chapman, J.B., 2017. Quantifying crustal thickness in continental collisional belts: global perspective and a geologic application. Sci. Rep. 7 https://doi.org/10.1038/s41598-017-07849-7.
Huang, W., 2014. Geochoronology, Geochemistry and origin of Carboniferous-Permian alkali granites in Eastern Tianshan, Hami, NW China. Master degree thesis. China University of Geosciences, Beijing, China.
Huang, Z.Y., Long, X.P., Kröner, A., Yuan, C., Wang, Y.J., Chen, B., Zhang, Y.Y., 2015. Neoproterozoic granitic gneisses in the Chinese Central Tianshan Block: implications for tectonic affinity and Precambrian crustal evolution. Precambrian Res. 269, 73–89.
Huang, Z.Y., Long, X.P., Wang, X.C., Zhang, Y.Y., Du, L., Yuan, C., Xiao, W.J., 2017. Precambrian evolution of the Chinese Central Tianshan Block: constraints on its tectonic affinity to the Tarim Craton and responses to supercontinental cycles. Precambrian Res. 295, 24–37.
Huang, B., Fu, D., Kusky, T., Ruan, K., Zhou, W., Zhang, X., 2018. Sedimentary provenance in response to Carboniferous arc-basin evolution of East Junggar and North Tianshan belts in the southwestern Central Asian Orogenic Belt. Tectonophysics 722, 324–341.
Huang, Z.Y., Yuan, C., Long, X.P., Zhang, Y.Y., Du, L., 2019. From Breakup of Nuna to Assembly of Rodinia: a link between the Chinese Central Tianshan Block and Fennoscandia. Tectonics. https://doi.org/10.1029/2018TC005471.
Huang, H., Wang, T., Tong, Y., Qin, Q., Ma, X.X., Yin, J.Y., 2020. Rejuvenation of ancient micro-continents during accretionary orogenesis: insights from the Yili Block and adjacent regions of the SW Central Asian Orogenic Belt. Earth Sci. Rev. 208, 103255.
Jahn, B.M., Wu, F.Y., Chen, B., 2000. Granitoids of the Central Asian Orogenic Belt and continental growth in the Phanerozoic. Trans. Roy. Soc. Edinburgh: Earth Sci. 91, 181–193.
Jahn, B.M., Windley, B., Natal'in, B., Dobretsov, N., 2004. Phanerozoic continental growth in Central Asia. J. Asian Earth Sci. 23, 599–603.
Kemp, A.I.S., Hawkesworth, C.J., Paterson, B.A., Kinny, P.D., 2006. Episodic growth of the Gondwana supercontinent from hafnium and oxygen isotopes in zircon. Nature 439, 580–583.
Kemp, A.I.S., Hawkesworth, C.J., Collins, W.J., Gray, C.M., Blevin, P.L., EIMF, 2009. Isotopic evidence for rapid continental growth in an extensional accretionary orogen: the Tasmanides, eastern Australia. Earth Planet. Sci. Lett. 284, 455–466.
Kogiso, T., Omori, S., Maruyama, S., 2009. Magma genesis beneath Northeast Japan arc: a new perspective on subduction zone magmatism. Gondwana Res. 16, 446–457.
Kröner, A., Kovach, V., Belousova, E., Hegner, E., Armstrong, R., Dolgopolova, A., Seltmann, R., Alexeiev, D.V., Hoffmann, J.E., Wong, J., Sun, M., Cai, K., Wang, T., Tong, Y., Wilde, S.A., Degtyarev, K.E., Rytsk, E., 2014. Reassessment of continental growth during the accretionary history of the Central Asian Orogenic Belt. Gondwana Res. 25, 103–125.

Kröner, A., Kovach, V., Alexeiev, D., Wang, K.L., Wong, J., Degtyarev, K., Kozakov, I., 2017. No excessive crustal growth in the Central Asian Orogenic Belt: further evidence from field relationships and isotopic data. Gondwana Res. 50, 135–166.
Lee, C.T., Morton, D.M., Kistler, R.W., Baird, A.K., 2007. Petrology and tectonics of Phanerozoic continent formation: from island arcs to accretion and continental arc magmatism. Earth Planet. Sci. Lett. 263, 370–387.
Lei, R.X., Wu, C.Z., Gu, L.X., Zhang, Z.Z., Chi, G.X., 2011. Zircon U–Pb chronology and Hf isotope of the Xingxingxia granodiorite from the Central Tianshan zone (NW China): implications for the tectonic evolution of the southern Altaids. Gondwana Res. 20, 582–593.
Li, W.Q., Ma, H.D., Wang, R., Wang, H., Xia, B., 2008. SHRIMP dating and Nd-Sr isotopic tracing of Kanggurtage ophiolite in eastern Tianshan, Xinjiang. Acta Petrol. Sin. 4, 773–780 (in Chinese with English abstract).
Li, X.H., Li, Z.X., Li, W.X., 2014. Detrital zircon U–Pb age and Hf isotope constrains on the generation and reworking of Precambrian continental crust in the Cathaysia Block, South China: a synthesis. Gondwana Res. 25, 1202–1215.
Li, H.D., Zhou, J.B., Wilde, S.A., 2022. Nature and development of the South Tianshan-Solonker suture zone. Earth Sci. Rev. 233, 104189.
Liu, W.G., Zhang, J.D., Zhao, H.L., 2016. Geological Characteristics and geochronology of Dongdagou oceanic crust remmants in Eastern Tianshan, Xinjiang. Western Explor. Eng. 6, 130–133 (in Chinese).
Liu, Y.J., Li, W.M., Ma, Y.F., Feng, Z.Q., Guan, Q.B., Li, S.Z., Chen, Z.X., Liang, C.Y., Wen, Q.B., 2021. An orocline in the eastern Central Asian Orogenic Belt. Earth Sci. Rev. 221, 103808.
Liu, H., Zhao, H., Guo, R., Wang, G., Liao, Q., 2022. Geochronology, geochemistry and geological implications of Early Carboniferous A-type granites in Harlik area from the Eastern Tianshan. Earth Sci. 47, 2245–2263.
Long, X.P., Huang, Z.Y., 2017. Tectonic affinities of microcontinents in the Central Asian Orogenic Belt: a case study of the Chinese Tianshan orogenic belt. Bull. Mineral. Petrol. Geochem. 36, 771–785 (in Chinese with English abstract).
Long, X.P., Yuan, C., Sun, M., Safonova, I., Xiao, W.J., Wang, Y.J., 2012. Geochemistry and U–Pb detrital zircon dating of Paleozoic graywackes in East Junggar, NW China: insights into subduction-accretion processes in the southern Central Asian Orogenic Belt. Gondwana Res. 21, 637–653.
Long, X.P., Wu, B., Sun, M., Yuan, C., Xiao, W.J., Zuo, R., 2020. Geochronology and geochemistry of Late Carboniferous dykes in the Aqishane-Yamansu belt, eastern Tianshan: evidence for a post-collisional slab breakoff. Geosci. Front. 11, 347–362.
Luo, T., Liao, Q.A., Chen, J.P., Zhang, X.H., Guo, D.B., Hu, Z.C., 2012. LA-ICP-MS zircon U–Pb dating of the volcanic rocks from Yamansu Formation in the Eastern Tianshan, and its geological significance. Earth Sci. J. China Univ. Geosci. 6, 1338–1352 (in Chinese with English abstract).
Luo, T., Liao, Q.A., Zhang, X.H., Chen, J.P., Wang, G.C., Huang, X., 2016. Geochronology and geochemistry of Carboniferous metabasalts in eastern Tianshan, Central Asia: evidence of a back-arc basin. Int. Geol. Rev. 58, 756–772.
Ma, J.C., 1999. Study on the Huangcaopo Group in the eastern Junggar. J. Mineral. Petrol. 19, 52–55 (in Chinese with English abstract).
Ma, X.X., Shu, L.S., Jahn, B.M., Zhu, W.B., Faure, M., 2012. Precambrian tectonic evolution of Central Tianshan, NW China: constraints from U–Pb dating and in site Hf isotopic analysis of detrital zircons. Precambrian Res. 222–223, 450–473.
Ma, X.X., Shu, L.S., Meert, J.G., 2015. Early Permian slab breakoff in the Chinese Tianshan belt inferred from the post-collisional granitoids. Gondwana Res. 27, 228–243.
Magni, V., 2019. The effects of back-arc spreading on arc magmatism. Earth Planet. Sci. Lett. 519, 141–151.
Mantle, G.W., Collins, W.J., 2008. Quantifying crustal thickness variations in evolving orogens: correlation between arc basalt composition and Moho depth. Geology 36, 87–90.
Mao, Q.G., Xiao, W.J., Fang, T.H., Windley, B.F., Sun, M., Ao, S.J., Zhang, J.E., Huang, X. K., 2014. Geochronology, geochemistry and petrogenesis of Early Permian alkaline magmatism in the Eastern Tianshan: implications for tectonics of the Southern Altaids. Lithos 190–191, 37–51.
Mao, Q.G., Yu, M.J., Xiao, W.J., Windley, B.F., Li, Y.C., Wei, X.F., Zhu, J.J., Lv, X.Q., 2018. Skarn-mineralized porphyry adakites in the Harlik arc at Kalatage, E. Tianshan (NW China): slab melting in the Devonian-early Carboniferous in the southern Central Asian Orogenic Belt. J. Asian Earth Sci. 153, 365–378.
Mao, Q.G., Wang, J.B., Xiao, W.J., Windley, B.F., Schulmann, K., Yu, M.J., Fang, T.H., Li, Y.C., 2019. Mineralization of an intra-oceanic arc in an accretionary orogen: insights from the early Silurian Honghai VMS Cu-Zn deposit and associated adakites of the Eastern Tianshan (NW China). Geol. Soc. Am. Bull. 131, 803–830.
Mao, Q.G., Wang, J.B., Yu, M.J., Ao, S.J., Li, Y.C., 2020. Re-Os and U-Pb geochronology for the Xiaorequanzi VMS deposit in the Eastern Tianshan, NW China: constraints on the timing of mineralization and stratigraphy. Ore Geol. Rev. 122, 103473.
Mao, Q.G., Ao, S.J., Windley, B.F., Song, D.F., Sang, M., Tan, Z., Wang, H., Li, R., Xiao, W.J., 2022a. Late Paleozoic Southward Migration of the Dananhu Arc in the Eastern Tianshan (NW China). Earth and Space. Science 9 e2021EA002027.
Mao, Q.G., Ao, S.J., Windley, B.F., Zhang, Z.Y., Sang, M., Tan, Z., Wang, H., Li, R., Xiao, W.J., 2022b. Middle-Late Triassic southward-younging granitoids: tectonic transition from subduction to collision in the Eastern Tianshan-Beishan Orogen (NW China). Geol. Soc. Am. Bull. 134, 2206–2224.
Mao, Q.G., Xiao, W.J., Buckman, S., Huang, P., Ao, S.J., Song, D.F., Zhang, J.E., Sang, M., Tan, Z., Wang, H., Li, R., 2022c. Deformational history of the Kanguer Subduction Complex in the Eastern Tianshan (NW China): implications for Paleozoic-Triassic multiple accretionary tectonics of the southern Altaids. Tectonics 41 e2022TC007527.
Pirajno, F., Seltmann, R., Yang, Y.Q., 2011. A review of mineral systems and associated tectonic settings of northern Xinjiang, NW China. Geosci. Front. 2, 157–185.
Profeta, L., Ducea, M.N., Chapman, J.B., Paterson, S.R., Gonzales, S.M.H., Kirsch, M., Petrescu, L., DeCelles, P.G., 2015. Quantifying crustal thickness over time in magmatic arcs. Sci. Rep. 5 https://doi.org/10.1038/srep17786.
Qin, K.Z., Su, B.X., Sakyi, P.A., Tang, D.M., Li, X.H., Sun, H., Xiao, Q.H., Liu, P.P., 2011. SIMS zircon U–Pb geochronology and Sr–Nd isotopes of Ni-Cu-bearing mafic–ultramafic intrusions in Eastern Tianshan and Beishan in correlation with flood basalts in Tarim basin (NW China): constraints on a ca. 280 Ma mantle plume. Am. J. Sci. 311, 237–260.
Reymer, A., Schubert, G., 1986. Rapid growth of some major segments of continental crust. Geology 14, 299–302.
Rudnick, R.L., Gao, S., 2014. 4.1 - Composition of the continental crust. In: Treatise on Geochemistry, Second edition, 4, pp. 1–51.
Rui, Z.Y., Wang, L.S., Wang, Y.T., Liu, Y.L., 2002. Discussion on metallogenic epoch of Tuwu and Yandong porphyry copper deposits in Eastern Tianshan Mountains, Xinjiang. Mineral Deposits 21, 16–22 (in Chinese with English abstract).
Sdrolias, M., Müller, R.D., 2006. Controls on back-arc formation. Geochem. Geophys. Geosyst. 7, Q04016.
Sengör, A.M.C., Natalin, B.A., 1996. Turkic-type orogeny and its role in the making of the continental crust. Annu. Rev. Earth Planet. Sci. 24, 263–337.
Sengör, A.M.C., Natalin, B.A., Burtman, V.S., 1993. Evolution of the Altaid Tectonic Collage and Paleozoic Crustal Growth in Eurasia. Nature 364, 299–307.
She, J.Z., Yang, W.Z., Qu, X., Jia, J., Di, X.C., 2017. Geochemistry and zircon U-Pb dating of the Dacaotanbei mafic-ultramafic complex, Eastern Tianshan and its geological significance. Bull. Mineral. Petrol. Geochem. 36, 82–91 (in Chinese with English abstract).
Shu, L.S., Zhu, W.B., Wang, B., Faure, M., Charvet, J., Cluzel, D., 2005. The post-collision intracontinental rifting and olistostrome on the southern slope of Bogda Mountains, Xinjiang. Acta Petrol. Sin. 21, 25–36.
Shu, L.S., Wang, B., Zhu, W.B., Guo, Z.J., Charvet, J., Zhang, Y., 2011. Timing of initiation of extension in the Tianshan, based on structural, geochemical and geochronological analyses of bimodal volcanism and olistostrome in the Bogda Shan (NW China). Int. J. Earth Sci. 100, 1647–1663.
Song, P., Tong, Y., Wang, T., Huang, H., Zhang, J., Huang, W., 2018. Zircon U-Pb ages, genetic evolution and geological significance of Carboniferous granites in the Harlik Mountain, East Tianshan, Xinjiang. Geol. Bull. China 37, 790–804.
Spencer, C.J., Murphy, J.B., Hoiland, C.W., Johnston, S.T., Mitchell, R.N., Collins, W.J., 2019. Evidence for whole mantle convection driving Cordilleran tectonics. Geophys. Res. Lett. 46, 4239–4248.
Su, C.Q., Jiang, C.Y., Xia, M.Z., Wei, W., Pan, R., 2009. Geochemistry and zircons SHRIMP U-Pb age of volcanic rocks of Aqishan Formation in the eastern area of north Tianshan, China. Acta Geol. Sin. 25, 901–915.
Su, B.X., Qin, K.Z., Sakyi, P.A., Li, X.H., Yang, Y.H., Sun, H., Tang, D.M., Liu, P.P., Xiao, Q.H., Malaviarachchi, S.P.K., 2011. U–Pb ages and Hf–O isotopes of zircons from Late Paleozoic mafic-ultramafic units in the southern Central Asian Orogenic Belt: tectonic implications and evidence for an Early-Permian mantle plume. Gondwana Res. 20, 516–531.
Sun, Y., Wang, J.B., Li, Y., Wang, Y.W., Yu, M.J., Long, L.L., Lv, X.Q., Chen, L., 2018. Recognition of Late Ordovician Yudai porphyry Cu (Au, Mo) mineralization in the Kalatag district, Eastern Tianshan terrane, NW China: constraints from geology, geochronology, and petrology. Ore Geol. Rev. 100, 220–236.
Sun, Y., Wang, J.B., Wang, Y.W., Long, L.L., Mao, Q.G., Yu, M.J., 2019. Ages and origins of granitoids from the Kalatag Cu cluster in Eastern Tianshan, NW China: constraints on Ordovician–Devonian arc evolution and porphyry Cu fertility in the Southern Central Asian orogenic belt. Lithos 330–331, 55–73.
Tang, G.J., Chung, S.L., Hawkesworth, C.J., Cawood, P.A., Wang, Q., Wyman, D.A., Xu, Y.G., Zhao, Z.H., 2017. Short episodes of crust generation during protracted accretionary processes: evidence from Central Asian Orogenic Belt, NW China. Earth Planet. Sci. Lett. 464, 142–154.
Tian, W.Q., Wang, P.J., Li, S.L., Sun, X.M., Wen, N., Liu, X., 2005. Petrography and geochemistry of the Middle Ordovician volcanic rocks of Daliugou Group in Hami wupu area of Eastern Tianshan, Xinjiang. J. Jilin Univ. (Earth Sci. Ed.) 3, 296–306.
Turner, S.P., Platt, J.P., George, R.M.M., Kelley, S.P., Pearson, D.G., Nowell, G.M., 1999. Magmatism associated with orogenic collapse of the Betic–Alboran domain, SE Spain. J. Petrol. 40, 1011–1036.
Wang, J.B., Wang, Y.W., He, Z.J., 2006. Ore deposits as a guide to the tectonic evolution in the East Tianshan Mountains, NW China. Geol. China 33, 461–469 (in Chinese with English abstract).
Wang, C.Y., Campbell, I.H., Allen, C.M., Williams, I.S., Eggins, S.M., 2009. Rate of growth of the preserved north American continental crust: evidence from Hf and O isotopes in Mississippi detrital zircons. Geochim. Cosmochim. Acta 73, 712–728.
Wang, C.Y., Campbell, I.H., Stepanov, A.S., Allen, C.M., Burtsev, I.N., 2011. Growth rate of the preserved continental crust: II. Constraints from Hf and O isotopes in detrital zircons from Greater Russian Rivers. Geochim. Cosmochim. Acta 75, 1308–1345.
Wang, B., Cluzel, D., Jahn, B.M., Shu, L.S., Chen, Y., Zhai, Y.Z., Branquet, Y., Barbanson, L., Sizaret, S., 2014. Late Paleozoic pre- and syn-kinematic plutons of the Kangguer-Huangshan Shear zone: inference on the tectonic evolution of the Eastern Chinese North Tianshan. Am. J. Sci. 314, 43–79.
Wang, Y.H., Zhang, F.F., Liu, J.J., Que, C.Y., 2016. Carboniferous magmatism and mineralization in the area of the Fuxing Cu deposit, Eastern Tianshan, China: evidence from zircon U–Pb ages, petrogeochemistry, and Sr–Nd–Hf–O isotopic compositions. Gondwana Res. 34, 109–128.
Wang, Y.F., Chen, H.Y., Han, J.S., Chen, S.B., Huang, B.Q., Li, C., Tian, Q.L., Wang, C., Wu, J.X., Chen, M.X., 2018. Paleozoic tectonic evolution of the Dananhu-Tousuquan island arc belt, Eastern Tianshan: constraints from the magmatism of the Yuhai porphyry Cu deposit, Xinjiang, NW China. J. Asian Earth Sci. 153, 282–306.

Wang, Y.H., Zhang, F.F., Xue, C.J., Liu, J.J., Zhang, Z.C., Sun, M., 2021. Geology and Genesis of the Tuwu Porphyry Cu Deposit, Xinjiang, Northwest China. Econ. Geol. 116, 471–500.
Wang, Y.J., Zhu, D.C., Lin, C.F., Hu, F.Y., Liu, J.G., 2022. Quantifying the growth of continental crust through crustal thickness and zircon Hf-O isotopic signatures: a case study from the southern Central Asian Orogenic Belt. Geol. Soc. Am. Bull. 134, 2072–2084.
Wang, T., Huang, H., Zhang, J.J., Wang, C.Y., Cao, G.Y., Xiao, W.J., Yang, Q.D., Bao, X. W., 2023. Voluminous continental growth of the Altaids and its control on metallogeny. Natl. Sci. Rev. 10 https://doi.org/10.1093/nsr/nwac283.
Wilhem, C., Windley, B.F., Stampfli, G.M., 2012. The Altaids of Central Asia: a tectonic and evolutionary innovative review. Earth Sci. Rev. 113, 303–341.
Windley, B.F., Allen, M.B., Zhang, C., Zhao, Z.Y., Wang, G.R., 1990. Paleozoic accretion and Cenozoic redeformation of the Chinese Tien Shan Range, Central Asia. Geology 18, 128.
Windley, B.F., Alexeiev, D., Xiao, W., Kröner, A., Badarch, G., 2007. Tectonic models for accretion of the Central Asian Orogenic Belt. J. Geol. Soc. Lond. 164, 31–47.
Wu, C.Z., Zhang, Z.Z., Zaw, K., Della-Pasque, F., Tang, J.H., Zheng, Y.C., Wang, C.S., San, J.Z., 2006. Geochronology, geochemistry and tectonic significances of the Hongyuntan granitoids in the Qoltag area, Eastern Tianshan. Acta Petrol. Sin. 22, 1121–1134 (in Chinese with English abstract).
Wu, B., Long, X.P., Zhang, S.T., Zhang, Y.Y., Huang, Z.Y., Du, L., 2022. Carboniferous variation of crustal thickness and subduction angles in Eastern Tianshan, NW China: evidence from the petrogenesis of the magmatic rocks in the Aqishan–Yamansu Belt. Int. Geol. Rev. 65, 682–705.
Xiao, W.J., Zhang, L.C., Qin, K.Z., Sun, S., Li, J.L., 2004. Paleozoic accretionary and collisional tectonics of the Eastern Tianshan (China): implications for the continental growth of Central Asia. Am. J. Sci. 304, 370–395.
Xiao, W.J., Han, C.M., Yuan, C., Sun, M., Lin, S.F., Chen, H.L., Li, Z.L., Li, J.L., Sun, S., 2008. Middle Cambrian to Permian subduction-related accretionary orogenesis of Northern Xinjiang, NW China: implications for the tectonic evolution of Central Asia. J. Asian Earth Sci. 32, 102–117.
Xiao, W.J., Huang, B.C., Han, C.M., Sun, S., Li, J.L., 2010. A review of the western part of the Altaids: a key to understanding the architecture of accretionary orogens. Gondwana Res. 18, 253–273.
Xiao, W.J., Windley, B.F., Allen, M.B., Han, C.M., 2013. Paleozoic multiple accretionary and collisional tectonics of the Chinese Tianshan orogenic collage. Gondwana Res. 23, 1316–1341.
Xiao, W.J., Windley, B.F., Sun, S., Li, J.L., Huang, B.C., Han, C.M., Yuan, C., Sun, M., Chen, H.L., 2015. A tale of amalgamation of three Permo-Triassic collage systems in Central Asia: oroclines, sutures, and terminal accretion. Annu. Rev. Earth Planet. Sci. 43, 477–507.
Xiao, B., Chen, H.Y., Hollings, P., Han, J.S., Wang, Y.F., Yang, J.T., Cai, K.D., 2017. Magmatic evolution of the Tuwu–Yandong porphyry Cu belt, NW China: constraints from geochronology, geochemistry and Sr–Nd–Hf isotopes. Gondwana Res. 43, 74–91.
Xie, W., Xu, Y.G., Chen, Y.B., Luo, Z.Y., Hong, L.B., Ma, L., Liu, H.Q., 2016. High-alumina basalts from the Bogda Mountains suggest an arc setting for Chinese Northern Tianshan during the Late Carboniferous. Lithos 256–257, 165–181.
Yang, G.X., Li, Y.J., Xiao, W.J., Tong, L.L., 2015. OIB-type rocks within West Junggar ophiolitic mélanges: evidence for the accretion of seamounts. Earth Sci. Rev. 150, 477–496.
Yang, Q., Wang, T., Guo, L., Tong, Y., Zhang, L., Zhang, J., Hou, Z., 2017. Nd isotopic variation of Paleozoic–Mesozoic granitoids from the Da Hinggan Mountains and adjacent areas, NE Asia: implications for the architecture and growth of continental crust. Lithos 272–273, 164–184.
Yuan, C., Sun, M., Wilde, S., Xiao, W.J., Xu, Y.G., Long, X.P., Zhao, G.C., 2010. Post-collisional plutons in the Balikun area, East Chinese Tianshan: evolving magmatism in response to extension and slab break-off. Lithos 119, 269–288.
Zhang, L.C., Liu, T.B., Shen, Y.C., 2002. Isotopic geochronology of the Late Paleozoic Kangguer gold deposits of the East Tianshan Mountains, Xinjiang, northwest China. Resour. Geol. 52, 249–261.
Zhang, D.Y., Zhou, T.F., Yuan, F., Fan, Y., Deng, Y.F., Xu, C., Zhang, R.F., 2014. Genesis of permian granites along the kangguer shear zone, jueluotage area, northwest China: geological and geochemical evidence. Lithos 198–199, 141–152.
Zhang, W.F., Chen, H.Y., Han, J.S., Zhao, L.D., Huang, J.H., Yang, J.T., Yan, X.L., 2016. Geochronology and geochemistry of igneous rocks in the Bailingshan area: implications for the tectonic setting of late Paleozoic magmatism and iron skarn mineralization in the eastern Tianshan, NW China. Gondwana Res. 38, 40–59.
Zhang, Y.Y., Yuan, C., Long, X.P., Sun, M., Huang, Z.Y., Du, L., Wang, X.Y., 2017. Carboniferous bimodal volcanic rocks in the Eastern Tianshan, NW China: evidence for arc rifting. Gondwana Res. 43, 92–106.
Zhang, Y.Y., Sun, M., Yuan, C., Long, X.P., Jiang, Y.D., Li, P.F., Huang, Z.Y., Du, L., 2018. Alternating trench advance and retreat: insights from Paleozoic magmatism in the Eastern Tianshan, Central Asian Orogenic Belt. Tectonics 37, 2142–2164.
Zhang, X.R., Zhao, G.C., Han, Y.G., Sun, M., 2019. Differentiating advancing and retreating subduction zones through regional zircon Hf isotope mapping: a case study from the Eastern Tianshan, NW China. Gondwana Res. 66, 246–254.
Zhang, Y.Y., Yuan, C., Sun, M., Long, X.P., Huang, Z.Y., Jiang, Y.D., Li, P.F., Du, L., 2020. Two late Carboniferous belts of Nb-enriched mafc magmatism in the Eastern Tianshan: heterogeneous mantle sources and geodynamic implications. Geol. Soc. Am. Bull. 132, 1863–1880.
Zhang, F.F., Wang, Y.H., Liu, J.J., Xue, C.J., Wang, J.P., Zhang, W., Li, Y.Y., 2022. Paleozoic magmatism and mineralization potential of the Sanchakou Copper Deposit, Eastern Tianshan, Northwest China: insights from Geochronology, Mineral Chemistry, and Isotopes. Econ. Geol. 117, 165–194.
Zhao, T.Y., Xu, S.Q., Zhu, Z.X., Liu, X., Chen, C., 2014. Geological and Geochemical Features of Carboniferous Volcanic Rocks in Bogda–Harlik Mountains, Xinjiang and Their Tectonic Significances. Geol. Rev. 60, 115–124 (in Chinese with English abstract).
Zhao, L.D., Chen, H.Y., Hollings, P., Han, J.S., 2019a. Late Paleozoic magmatism and metallogenesis in the Aqishan-Yamansu belt, Eastern Tianshan: constraints from the Bailingshan intrusive complex. Gondwana Res. 65, 68–85.
Zhao, L.D., Chen, H.Y., Hollings, P., Han, J.S., 2019b. Tectonic transition in the Aqishan-Yamansu belt, Eastern Tianshan: constraints from the geochronology and geochemistry of Carboniferous and Triassic igneous rocks. Lithos 344–345, 247–264.
Zhao, H., Liao, Q.A., Li, S.Z., Xiao, D., Wang, G.C., Guo, R.L., Xue, Z.Q., Li, X.Y., 2022. Early Paleozoic tectonic evolution and magmatism in the Eastern Tianshan, NW China: evidence from geochronology and geochemistry of volcanic rocks. Gondwana Res. 102, 354–371.
Zhou, T.F., Yuan, F., Zhang, D.Y., Fan, Y., Liu, S., Peng, M.X., Zhang, J.D., 2010. Geochronology , tectonic setting and mineralization of granitoids in Jueluotage area , eastern Tianshan, Xinjiang. Acta Petrol. Sin. 26, 478–502 (in Chinese with English abstract).